JOURNAL OF MULTIFUNCTIONAL MATERIALS & PHOTOSCIENCE
9(2), December 2018, pp. 241-282

Photocatalytic CO_2 Reduction with Graphene-semiconductor

Zambaga Otgonbayar, Won-Chun Oh[1*] and Chang Sung Lim[**]

Department of Advanced Materials Science & Engineering, Hanseo University, Chungnam 356-706, South Korea

Abstract: Photocatalytic CO_2 reduction to solar fuel production is of tremendous importance as it has the potential for solving energy and global warming problems simultaneously. A number of reports have already been published on several novel and efficient photocatalysts for CO_2 reduction. Graphene, a two-dimensional material, owing to its large surface area, high conductivity, ease of functionalization , superior chemical stability and low cost, has emerged as an efficient photocatalyst for CO_2 reduction. Furthermore, graphene oxide or reduced graphene oxide materials can be coupled with various semiconductors to form hybrid nanocomposites, which can act as superior visible light active photoredox catalysts owing to their enhanced quantum efficiency. Coupling of graphene with a semiconductor can provide the photocatalyst with several advantages, including large surface area, abundant surface active sites, enhanced adsorption capacity, and a high electron hole separation rate. This article mainly focuses on the recent important advances in the application of graphene-based photocatalysts for CO_2 reduction to solar fuels.

Keyword: Graphene, Semiconductor, CO_2 reduction, Photocatalyst, Bandgap

1. Introduction

Fast growing scientific developments are providing abundant conveniences to human society and instigating the profligate use of energy resources. It has been anticipated that the world energy demands may rise by 28% by 2040 [1]. Currently, most of the energy requirements are fulfilled by the combustion of fossil fuels such as coal, oil and natural gas [2] and if this trend persists, available fossil fuels reservoirs could be depleted in future [3]. Additionally, excessive combustion of fossil fuels is the main cause of global warming and threatening the ecosystem due to increasing level of greenhouse gas, CO_2. It has been anticipated that CO_2 level could reach to 750 ppm from its normal value of 400 ppm (0.04%) and global temperature may rise by 10–15 °F [4,5]. Hence, development of sustainable renewable energy resources is highly demanding to provide energy and control the global warming. Owing to the depletion of fossil fuels and increasing emission of CO_2, the exploration of clean and renewable energy has received much attention.

* Corresponding author: *wc_oh@hanseo.ac.kr; cslim@hanseo.ac.kr*

Photocatalytic CO_2 reduction is known as one of the most promising renewable energy technologies for overcoming the aforementioned problems because of its ability to convert CO_2 to valuable solar fuels such as CH_4, HCO_2H, CH_2O, and CH_3OH by utilizing solar energy [6], [7], [8], [9], [10]. Since the break through work on the photocatalytic CO_2 reduction by Inoue *et al*. [11], numerous reports have been published on the preparation of highly efficient photocatalysts to meet the practical requirements of the photocatalytic systems for CO_2 reduction [12], [13]. However, photocatalytic CO_2 reduction is still limited by its low solar conversion efficiency because of the fast recombination of photoinduced electrons and holes, slow charge consumption during reduction–oxidation (REDOX) reaction and low light utilization [14], [15], [16]. To this end, the preparation of highly efficient photocatalysts with slow electron–hole recombination, fast charge consumption during REDOX reaction and good light utilization are the key challenges to improve the photocatalytic CO_2 reduction performance.

Several techniques have been utilized for the reduction of CO_2 such as carbon capturing and storage (CCS), electrochemical and thermochemical conversion, catalytic conversion, photo electrochemical, biological fixation and photocatalytic reduction [17,18]. The CCS is extensively researched techniques with remarkable efficiency but environmental risk of leakage from geological storages, cost of compression and transportation have constrained its wide applications [19]. Similarly, electrochemical technique reduces CO_2 into value added chemicals using high power electrical energy, however, lower efficiency and electrode stability limit the process efficiency [20]. Likewise, the biological transformation of CO_2 into useful products bymicroalgae suffers from the limitations of production and regeneration of enzymes [21]. In addition, thermal and catalytic conversion of CO_2 into methane (CH_4) and carbon monoxide (CO) using transition metals catalysts is an efficient method for practical applications. Nevertheless, due to high temperature, pressure and exothermic reactions, capital and operational cost of process is high [22]. Photocatalytic technique, artificial photosynthesis, is the conversion of CO_2 and water into solar fuels like CH_4, CO, methanol (CH_3OH), formic acid (HCOOH) and formaldehyde (HCHO) under solar light irradiations. Among them, photocatalytic CO_2 reduction is the best process due to economical reactant (water), abundantly available solar energy, no toxic product or residue, and zero carbon emission [23]. Therefore, solar fuel generation from CO_2 through artificial photosynthesis process seems to be the most economical and eco-friendly approach for sustainable development. Since first report by Inove and Fujishima *et al*. [24], intense efforts have been done to enhance the efficiency of photocatalytic CO_2 reduction. Various photocatalysts including zinc oxide (ZnO) [25], tungsten oxide (WO_3) [26], gallium phosphide (GaP) [27], gallium oxide (Ga_2O_3) [28], zirconium oxide (ZrO_2) [29], zinc sulfide (ZnS) [30], cadmium sulfide (CdS) [31], bismuth sulfide (Bi_2S_3) [32], lead selenide (PbSe) [33], graphitic carbon nitride (g-C_3N_4) [34] and titanium dioxide (TiO_2) [35] have been employed for photocatalytic degradation of CO_2. Among all, TiO_2 is broadly studied photocatalyst due to its unique properties, high chemical stability, availability and non-toxicity. Nevertheless, TiO_2 shows good activity under UV light irradiations and suffers from surface charge recombination problem [[36], [37], [38]]. Several strategies have been employed to enhance the

performance of TiO_2-based photocatalysts such as surface modifications, heterojunction, doping with metals and non-metals, surface plasmons, morphologies, and other techniques to enhance the uptake of CO_2 [[39], [40], [41], [42], [43]]. Besides limitations of photocatalyst, fundamentals aspects such as reaction mechanism, selectivity of solar products, mass transfer and thermodynamics of photocatalytic CO_2 reduction are not well established. The objective of this study is to summarize the current progress on TiO_2-based photocatalytic CO_2 reduction system. Fundamentals aspects such as thermodynamics, mass transfer, selectivity and reaction mechanism of CO_2 reduction are critically deliberated and illustrated with examples from other research studies. In the main stream, various strategies that have been reported to overcome the problems of TiO_2-based photocatalysts like photosensitizations, doping with metals and non-metals, heterojunctions, surface plasmons, novel architectures, functionalized surfaces, and state of the art morphologies have been analyzed and elaborated. Great emphasis has been devoted to the graphene modified TiO_2 composites due to peculiar features of graphene. Particularly, role of the graphene as a supporting material, electron acceptor, electron mediator in Z-scheme structures, surface plasmons of graphene, bandgap reduction, high surface area and delocalized π-conjugated electronic structure have been discussed and illustrated in detail.

2. Synthesis of Graphene materials

Graphene is a suitable candidate to anchor on the surface of semiconductor materials and promote the charge transfer mechanism. The discovery of graphene by Andre Geim and Konstantin Novoselov in 2004 has motivated the scientific community to explore extensively the potential applications of this material [44]. Graphene is commonly referred as a two dimensional (2D) sheet-like material with sp^2 hybridized carbon atoms configured in a hexagonal or honeycomb-like structure and its thickness is equivalent to an atom diameter [45]. Furthermore, graphene is made up of pure carbon whereby each carbon atom is covalently bonded together in the same planar and the monolayer graphene sheets are linked by van der Waals forces. Along with its derivatives, particularly graphene oxide (GO) and reduced graphene oxide (rGO), graphene materials have been studied in various fields due to the presence of aromatic ring, free π-π electron and reactive functional groups. A number of comprehensive reviews have documented the remarkable performance of graphene materials [46], [47], [48], [49]. For instance, Zhao et al. [50] developed an S-doped graphene sponge for the removal of Cu^{2+} with a high adsorption capacity of 228 mg/g which was 40 times greater than activated carbon. Mechanical properties enhancement by graphene material has been proven in Yang's work [51].

The number of graphene related research articles and patents has increased rapidly in the past 5 years suggesting the blooming era of graphene and the statistics are expected to increase in the upcoming years [52], [53]. At present, the graphene synthesis methods can be classified into two groups, namely top-down method and bottom-up method. The top-down approach involves the structural breakdown of precursor such as graphite followed by the interlayer separation to produce graphene sheets. Some examples of this method include mechanical exfoliation, oxidation–reduction of GO, liquid phase exfoliation and

arc discharge. Meanwhile, the bottom-up technique such as chemical vapor deposition, epitaxial growth and total organic synthesis utilize carbon source gas to synthesize graphene on a substrate. Graphene has emerged as one of the most interesting carbon nanomaterials since its successful isolation from graphite in 2004 [54]. Hence, GO is a compound structurally rich in carbon, hydrogen and oxygen. Since there are different methods to synthesize GO, its non-stoichiometric structure and composition are highly dependent on the production step [55]. Therefore, several structures of GO have been proposed, namely the Hofmann, Ruess, Scholz-Boehm, Nakajima-Matsuo, Lerf-Klinowski

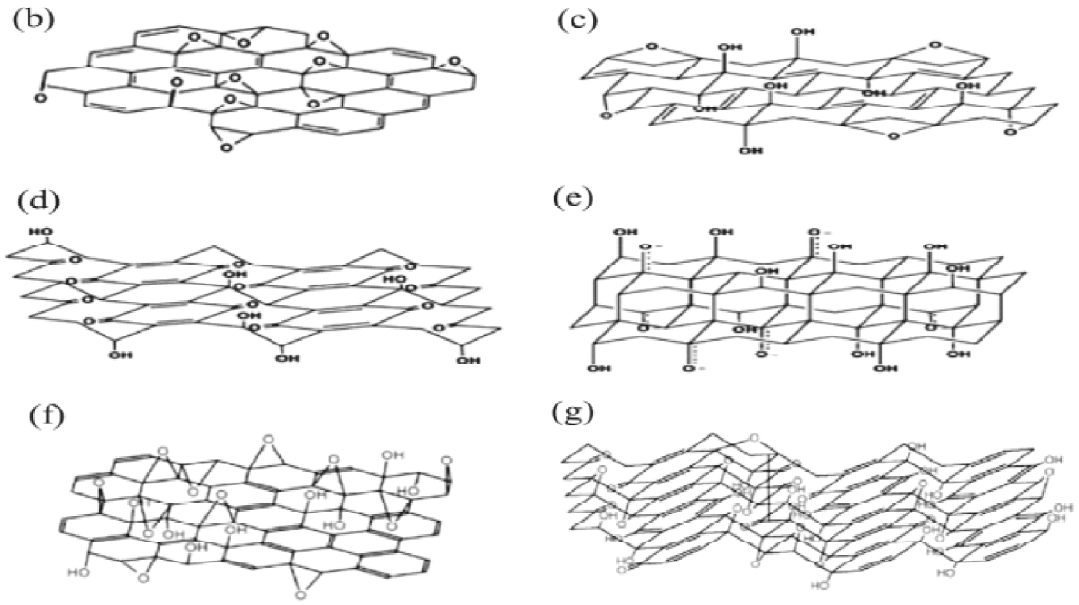

Figure 1: (b), Ruess (c), Scholz-Boehm (d), Nakajima-Matsuo (e), Lerf-Klinowski (f) and Szabo (g) models [57].

and Szabo models [56] as illustrated in Fig. 1(b)–(g).

The synthesis of graphene can be performed by two main approaches: top-down (destruction) and bottom-up (construction) methods [58], [59] . The top-down methods such as mechanical exfoliation [60], arc discharge [61], oxidative exfoliation-reduction [62], [63], liquid-phase exfoliation (LPE) [64], [65] and unzipping of CNT [66], [67] usually isolate and delaminate the layers of graphite into single-, bi- and few-layer graphene. These methods destroy larger precursors such as graphite and other carbon-based precursors to form nano-sized graphene. The bottom-up methods include chemical vapor deposition (CVD) [68], [69], epitaxial growth [70], [71], substrate-free gas-phase synthesis (SFGP) [72], template route [73] and total organic synthesis [74]. Even though the bottom-up methods produce graphene products with almost defect-free and large surface area, they often involve high production cost and sophisticated operational setup.

2.1. Mechanical exfoliation

One of the recent studies on the normal force synthesis route is the peeling of graphite using advanced machinery of ultra-sharp single crystal diamond wedge [75]. This method eliminates the need for manual operation, and saves time and labor cost. Another method uses a three-roll mill machine, an established technique in rubber industry, to produce graphene of 1.13–1.41/ nm [76], [77].

2.2. Oxidative exfoliation-reduction

Most GO are synthesized by oxidative exfoliation of graphite followed by reduction to graphene sheets or rGO. There are four main routes for GO synthesis which include those of Brodie, Staudenmaier, Hofmann and Hummers. Fig. 2 shows the reaction pathways of these methods which occur at temperatures below 100°C [78], [79]. The relatively low synthesis temperature is desirable to maintain low production cost. However, toxic gases such as nitrogen dioxide (NO_2) and di-nitrogen tetroxide (N_2O_4) are generated by these methods [80], [81]. Currently, the Hummers method is widely used for synthesis of GO as it is a comparatively fast and safe process. Moreover, it does not generate explosive gases such as chlorine dioxide (ClO_2) and acidic fog with the use of potassium permanganate ($KMnO_4$) and sodium nitrate ($NaNO_3$) instead of potassium perchlorate ($KClO_4$) and nitric acid (HNO_3) [82]. Over the years, modification of the Hummers method has introduced a greener approach to producing GO [83]. For instance, the improved Hummers method has eliminated the use of $NaNO_3$ to synthesize GO, thereby decreasing the production cost and environmental protection cost [84].

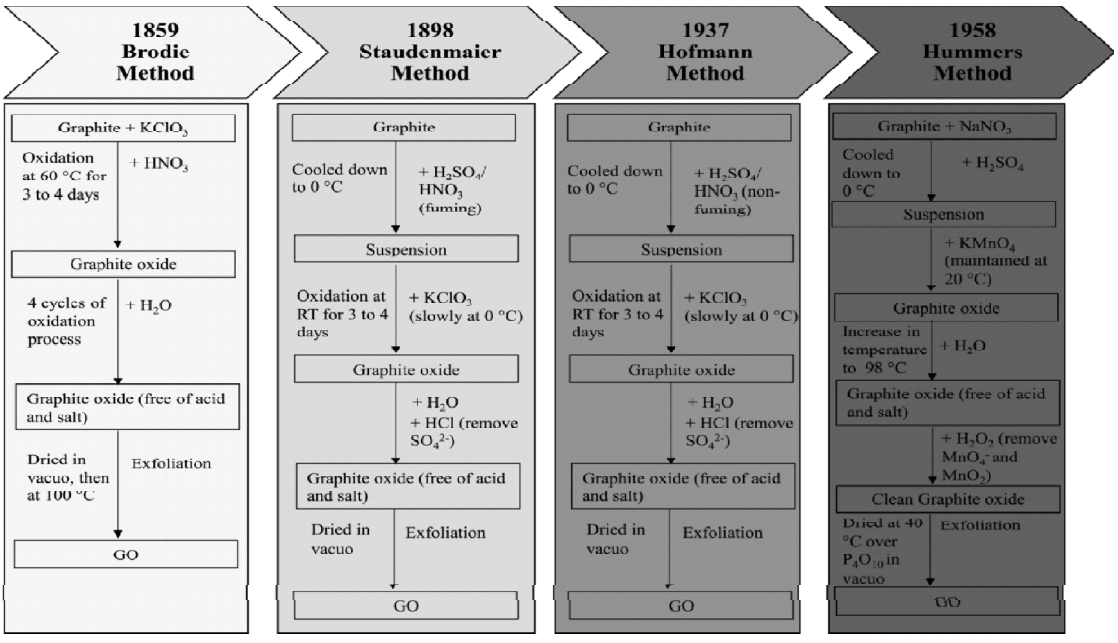

Figure 2: Graphite oxidation route schemes [85], [86].

2.3. *Chemical vapor deposition (CVD)*

CVD decomposes hydrocarbon gases (such as methane (CH_4), acetylene (C_2H_2), ethylene (C_2H_4) and hexane (C_6H_{14})) and other biomass materials to grow graphene sheet on metallic catalysts (such as Cu and Ni films) at elevated temperatures (650–1000°C) [87], [88]. CVD can produce high quality graphene with low defects, highly interconnected structure and large surface area [89]. Many researchers have focused on optimizing the synthesis conditions at lower temperature and ambient pressure, without compromising the quality of graphene [90], [91]. For instance, Kalita *et al.* [92] were able to synthesize graphene coating at 450°C using surface wave plasma enhanced CVD (PECVD). This procedure significantly lowered the growth temperature and deposition time (< 5 min) which subsequently enhanced the overall synthesis and scalability of the process [93]. The setup of conventional CVD can be modified into PECVD.

2.4. *Epitaxial growth*

Graphene can also be prepared by thermal decomposition (1200–1600°C) of hexagonal substrate (silicon carbide (SiC)) under vacuum or inert condition [94]. High temperature treatment causes silicon (Si) to sublimate (Si melting point/ =/ 1100°C), leaving excessive C atoms to aggregate and form an sp^2 hybridized network which induce graphene growth [95]. This process is known as epitaxial growth of graphene on SiC [96], [97]. Based on current synthesis condition, epitaxial growth of graphene would be expensive due to the energy intensive process and limited size of commercial SiC substrate [98]. Furthermore, the epitaxial growth can produce different polar faces such as Si-face or C-face which hinder the graphene product quality [99], [100]. Si-face graphene formation is preferred as it ensures homogeneous growth of graphene [101]. Using this method, the number of layers of graphene which depends on heating temperature can be easily modulated [102]. So far, this synthesis method is still under review as data on the growth mechanisms and interaction between graphene and the substrate is still scarce [103].

3. Synthesis of Graphene - semiconductor

Combining semiconductors and carbon to form composite materials is expected to environmental pollution to a certain extent, so these photocatalytic materials are worth exploring. Carbon materials including graphite, carbon black, activated carbon, carbon fibers, carbon nanotubes (CNTs), and fullerenes [104,105] have been combined with semiconductors. Graphene is another type of carbon material, and is composed of a single layer of sp2 bonded carbon atoms, as shown in the scanning electron microscope (SEM) image and schematic diagram in Fig. 3.

The basic construction unit of Graphene is the stable benzene ring with a monolayer thickness of 0.35 nm [106]. Graphene is the basic unit in numerous carbon materials including graphite, carbon nanotubes, and fullerenes [107–109]. Compared with carbon nanotubes and fullerenes, graphene has higher conductivity and chemical stability, and improved mechanical properties. Furthermore, the unique two dimensional planar structure and high specific surface of GR mean that it shows great potential as a carrier

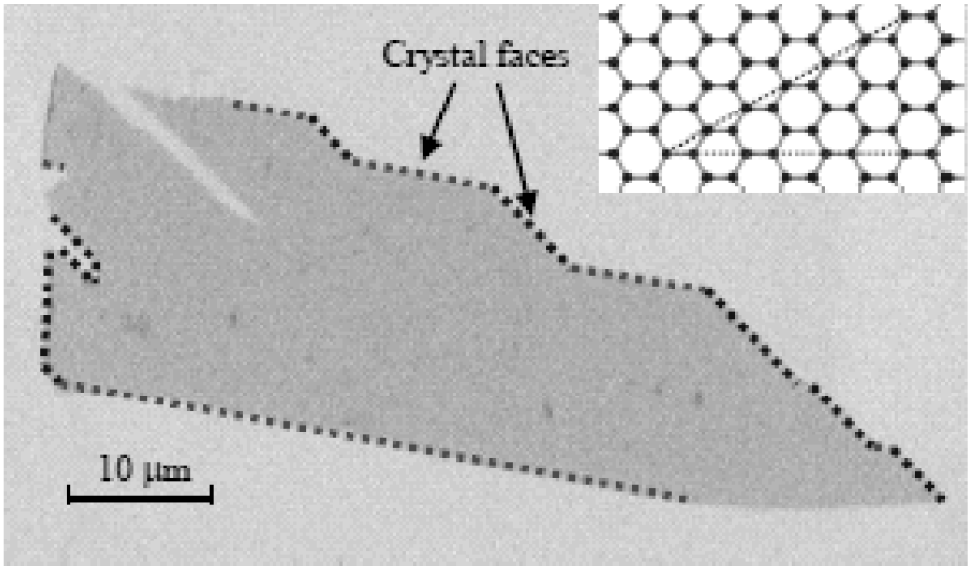

Figure 3: SEM image and schematic diagram of the atomic structure of Grapheme (GR)

and multifunctional material for transferring electrons and holes. Semiconductor/graphene composite photocatalysts have been a hot topic of research in recent years. A number of methods do exist allowing for the GR-semiconductors composites with diverse morphology, size, dimensionality and interfacial domains [110], all affecting the efficiency of the photocatalytic processes. However, all the synthetic techniques producing GR conjugated composites can be categorized into: in-situ *crystallization* and *ex-situ hybridization* [111].

3.1. In-situ method

In-situ crystallization, this is the most common method. In-situ methods including sol-gel method, hydrothermal/solvothermal treatment, and microwave-assisted deposition have been exploited to fabricate GR based composites through a one-step growth or by a multi-step reaction procedure. In this method based on a the direct and homogenous growth of nanomaterials (such as nanoparticles, nanowires, nanorods, nanotubes or nanofilms) on the surface of a GR precursor, mainly GO or RGO [112]. In-situ crystallization is based on mixing GO or RGO and the soluble precursors of the inorganic semiconductors in a solvent, following a chemical, thermal, optical or ultrasonic treatment of the mixture to finally anchor the inorganic catalysts on the surface of GR. The oxygen sites of GO act as nucleation points for the adjustment of size, morphology and crystallinity of the nanoparticles and enable the efficient interfacial contact of nanomaterials on GO/RGO surface to improve the efficiency of electron transfer.

3.1.1. Sol-gel method

A wet chemical approach, is based on phase transition from a precursor, a colloidal liquid, into a solid gel through a series of hydrolysis and polycondensation reactions. Its

key advantage is the effective anchoring of the catalyst at the OH groups of GO/RGO by chemical bonding. The precursors used in the preparation of GR-semiconductor composites are mostly metal alkoxides, metal chlorides, and organometallic compounds. As an example, in the fabrication of TiO_2-RGO or GO composite photocatalysts via a sol-gel method, the precursors used were titanium tetra-isopropoxide (TTIP) [113], [114], [115], titanium butoxide (TBOT) [116], [117], [118], [119], [120], and titanium tetrachloride ($TiCl_4$) [121], which resulted in different structures of TiO_2 depending on the experimental conditions applied. From TTIP the following steps produced a composite catalyst:

$$GO_xH_y + (CH(CH_3)_2O)_4Ti \xrightarrow{O_2, C_3H_7OH, unbalanced} \{CH(CH_3)_2 - O)_3Ti - O\} \quad (1)$$

$$\{CH(CH_3)_2 - O)_3Ti - O\} - G \xrightarrow{O_2, 300°C, 2h, unbalanced} (TiO_2) - G + CO_2 \quad (2)$$

Final drying and annealing at temperatures typically above 300 °C resulted in semiconductor photocatalysts, whose crystallinity and photocatalytic activity were strongly affected by the final heat treatment. Studies on the structural integrity of GR-inorganic semiconductor composites have been conducted by Chun *et al.* [122], who found out that a high temperature up to 400 °C in the final treatment enhances the photocatalytic activity of TiO_2-3% (w/w) GO without significantly affecting its structural features.

3.1.2. Hydrothermal/solvothermal method

In this method widely used for the fabrication of composite photocatalysts, based on crystallization of catalysts on GO sheets with the simultaneous reduction of GO at high temperature and pressure. It can take place with or without reductants starting from an aqueous/alcoholic solution [123], [124], [125], [126]. Sher Shah *et al.* [127] synthesized Ag-TiO_2-RGO, a ternary nanocomposite photocatalyst, by dispersing TTIP in N,N dimethyl formamide (DMF) and ethylene glycol (EG) containing silver nitrate and RGO to reduce silver nitrate to silver and mitigate the agglomeration of RGO nanosheets upon treatment at 200 °C for 18 h, as illustrated in Fig. 4. The resulting Ag and TiO_2 nanoparticles were evenly distributed on RGO sheets without agglomeration of RGO. During the fabrication of GR-semiconductor photocatalysts, Liu *et al.* [128] targeted different exposed facets of TiO_2, namely {101}, {100}, and {001}, to be grown on GR through a hydrothermal reaction by capping anions at 180 °C for 24 h. After a through structural and physicochemical analysis, they reported that directionality on the facet growth also affected the photocatalytic activity by changing the bonding structure of GR and TiO_2, and thus the interfacial charge transfer rates.

3.1.3. Microwave-assisted synthesis

In this method is a fast and low temperature method of producing GR-inorganic semiconductors composites compared to other in situ procedures. This technique enables to induce nucleation and growth of small and homogenous particles on GR [129]. UV microwave-assisted technique was used during the fabrication of OH-TiO_2/RGO by UV

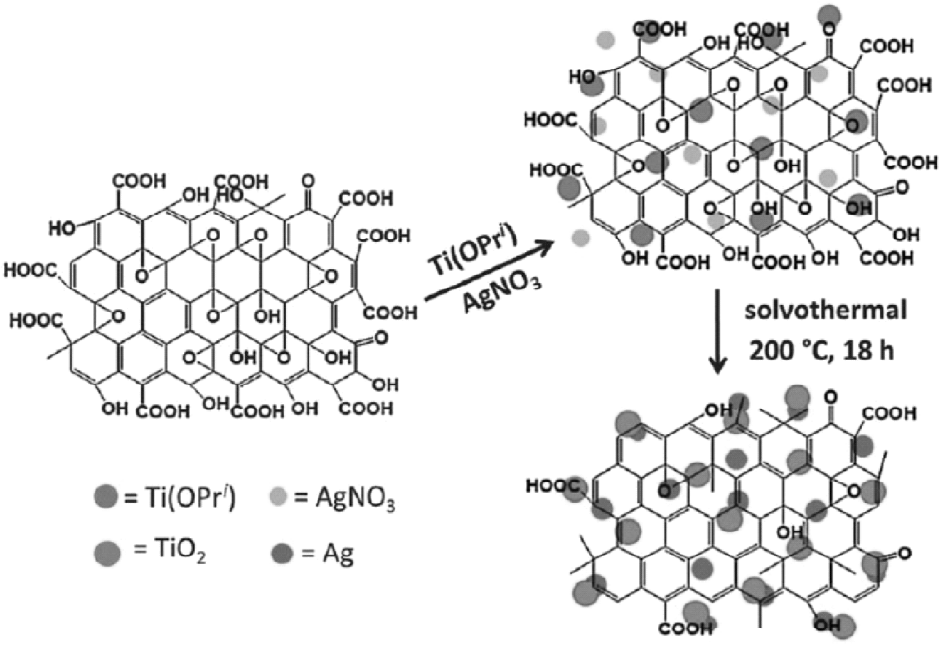

Figure 4: Fabrication of Ag-TiO_2-RGO ternary nanocomposite photocatalyst

irradiation of their precursors, i.e. TBOT and GO, and treating them through microwaves [130]. The results indicated that surface hydroxylation on RGO/TiO_2 catalyst enabled extension of visible light absorption up to about 600 nm with a color shift to yellow, at the same time reducing crystal sizes, inducing surface defects such as Ti^{3+} states and oxygen vacancies, thereby enhancing charge transfer with a lower recombination rate. All reviewed studies on in situ synthesis suggest that GO is the most used precursor of GR because of its high degree of hydrophilic functional groups that allows for water process ability.

3.2. Ex-situ hybridization

Ex-situ hybridization, such as a ex-situ method is based on mixing nanomaterials with a defined structure and composition with GR precursors, aiming to anchor the inorganic particles to oxygen moieties existing at the surface of GO or RGO via covalent or noncovalent interaction [131]. For instance, coating GO sheets on a Nb-doped TiO_2 (TNO) thin film resulted in a transparent conducting oxide (TCO) layer fabricated by a self-assembly technique, and being indium free, low cost and enhancing charge transport. According to the photocatalytic activity measurement, GO on TNO films exhibit an improved photocatalytic efficiency on degradation of methylene blue (MB) [132].

3.2.1. Self-assembly technique

In self-assembly technique, the distribution of nanomaterial on GR is random. For this

reason, to maximize unique properties of GR, the surface modification of either GR or the inorganic semiconductors is necessary to improve their ability to process solvent, and to increase the spatial interaction between GR and the catalysts [133]. Xiao *et al.* [134] constructed 2% RGO/SiO_2 hollow microsphere composites via ultrasound-assisted interfacial self-assembling of negatively charged GO sheets on positively charged SiO_2 modified with poly-(diallyldimethylammonium) chloride (PDDA). Sonication enabled the composite to disperse in the aqueous solution thus preventing aggregation. The following solvothermal treatment resulted in a further reduction of GO and better interfacial contact between SiO_2 and RGO. Another approach involves the aerosol assisted self-assembly method, which is simple, low cost and easy to scale up, allowing to achieve a charge transfer between TiO_2 and RGO sheets and to foster interfacial contact between TiO_2 and RGO compared to the electrostatic assembly approach [135]. From the perspective of synthesizing composites with robust interfacial contact between inorganic catalysts and GR, the ex-situ synthesis method is often less efficient than in-situ. The stronger interfacial interactions can be attributed to the generation of chemical bonds which tends to foster the effective separation of electron-hole pairs with an efficient electron transfer and the narrowing of optical band gaps. Conversely, we want to highlight that the advantage of ex-situ method is to the control of the morphology of the materials into ordered and monodisperse structures by pre-selection of semiconductors with desirable morphology. In the course of ex-situ preparations, the shape, size and morphology of the used semiconductors in the composites are nearly the same as the initial ones. A fair comparison of the photoactivity of the composites with respect to inorganic semiconductors is then feasible, without any concern on the morphological structure influence.

4. Dimensionality of composites

Besides doping/co-doping techniques to modulate the carrier separation and transfer of GR-semiconductor, several studies indicated that the photocatalytic performance of GR-semiconductor composites are also improved by tuning surface area, mass transfer kinetics and local assembly environment, since these parameters have a synergistic effect on the whole photocatalytic reactions. Zero-dimensional (0D), nanoribbons, nanotubes, nanowires and nanorods, belonging to the one-dimensional (1D) category, single-atom thick material like sheets being two-dimensional (2D) and, finally, nanospheres and nanocones, which are among the 3D morphologies. Dimensionality can explain the atomic assembly of the materials and also affect their properties to a significant degree. The same component can exhibit a very different photocatalytic activity when existing in different shapes, due to a different charge mobility and reduced recombination resulting in a prolonged charge life and shorter transfer paths.

4.1. Two-dimensional structures

The dimensionality of each component of a composite and the increased interfacial contact area are able to enhance the electron transfer thus result in a better photocatalytic activity. Coupling of lower dimensional structures and GR such as in 0D/2D, 1D/2D

and 2D/2D hetero structures, is an effective way for boosting the global photocatalytic performance [89].

In 0D/2D and 1D/2D composites, nanoparticles, nanorods, nanowires or nanotubes have been coupled with GR through in-situ growth methods or ex-situ assembly. However, 2D/2D hetero structures have better interfacial contact areas due to the more efficient face-to-face contact, which enhances the photocatalytic performance by increasing the electron transfer and separation of photogenerated electron-hole pair compared to 0D/2D, where inorganic semiconductors are dispersed on 2D GR sheets, either homogeneously or wrapped inside nanosheets, and also compared to 1D/2D configurations, where a line-to-line interaction occurs as shown in Fig. 5 [136]. A 2D/2D arrangement has been described for instance by Luan *et al.* [137], who indicated that

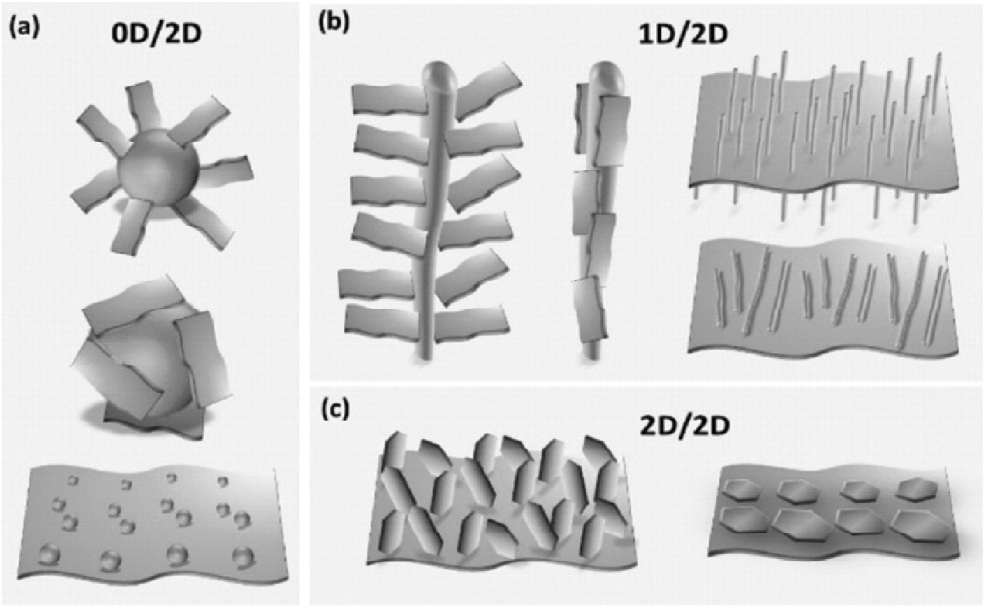

Figure 5: GR based composites with different dimensionality and interfacial contacts

the usage of 2D TiO_2 nanosheets in the fabrication of GR-modified semiconductor catalysts has advantages, serving as a hosting material to load guest functional nanomaterials, providing a large interaction area between catalyst and organic pollutant.

4.2. Three-dimensional structure

GR, with its unique 2D structure, can be used as the building block for the self-assembly of 3D functional materials. Due to the strong interaction among GR sheets, it is hard to dissolve GR in most solvents. However, in a gel medium, it can be well dispersed thanks to the covalent π–π stacking interactions with a gelator peptide [138]. Moreover, when

synthesized by Hummer method, GO is soluble in water yielding a homogenous liquid which is beneficial for the 3D self-assembly procedures, producing organo-gels, aerogels, and hydrogels. The 3D structures obtained, for instance, in porous films, aerogels, and scaffolds, allow GR to enhance specific surface area, charge carrier transfer and conductivity, and to inhibit aggregation, by means of combination of 3D porous structure and the peculiar properties of GR, namely high surface area, high conductivity and electron mobility. Among the several 3D structures of GR which have been reported, GR hydrogels/aerogels have attracted widespread attention due to (i) the porous structure providing an ideal support to fabricate photocatalytic semiconductors, (ii) the shapes, volumes and densities adaptability, allowing for high adsorption ability, and (iii) the affordable and convenient recycling of the photocatalysts due to the prompt separation from the reaction media. As an example, a study focused on construction of 3D porous aerogel constituted by GR sheets and Bi_2WO_6 nanosheets, indicated that the bi-component photocatalyst achieved higher degradation of rhodamine B(RhB) compared to bare Bi_2WO_6, due to a 60% higher specific surface area and higher adsorption of RhB compared to bare Bi_2WO_6 sheets [93]. GO/polymer hybrid microspheres were fabricated by getting 2D GO sheets wrapped on the surface of polymer microspheres and assembled into 3D structures [94]. The wrinkled surface of the photocatalyst increased the specific surface area and allowed the particles to grow on 3D structures by providing effective sites [139]. The photocatalytic activity of TiO_2/RGO/polymer composites on the degradation of RhB under visible light was about 96% in 30 min, much better compared to TiO_2 Degussa P25, owing to the good crystallinity and the small size of anatase TiO_2 particles, the unique electrical conductivity of GR, and the interactions between TiO_2 and RGO in this complex composite.

5. Semiconductor

A semiconductor is a substance, usually a solid chemical element or compound, that can conduct electricity under some conditions but not others, making it a good medium for the control of electrical current. Its conductance varies depending on the current or voltage applied to a control electrode, or on the intensity of irradiation by infra-red (IR), visible light, ultraviolet (UV), or X rays.

Semiconductors are typically:

- Stoichiometric: elemental, binary, tertiary, quaternary,
- Crystalline - small band gap materials Ω semiconducting
- Covalently bonded (mainly)

The specific properties of a semiconductor depend on the impurities, or *dopants*, added to it. Properties of semiconductor:

1. Variable electrical conductivity: Semiconductors in their natural state are poor conductors because a current requires the flow of electrons, and semiconductors have their valence bands filled, preventing the entry flow of new electrons. There are several

developed techniques that allow semiconducting materials to behave like conducting materials, such as doping or gating. These modifications have two outcomes: n-type and p-type. These refer to the excess or shortage of electrons, respectively. An unbalanced number of electrons would cause a current to flow through the material [146].

2. Heterojunctions: Heterojunctions occur when two differently doped semiconducting materials are joined together. For example, a configuration could consist of p-doped and n-doped germanium. This results in an exchange of electrons and holes between the differently doped semiconducting materials. The n-doped germanium would have an excess of electrons, and the p-doped germanium would have an excess of holes. The transfer occurs until equilibrium is reached by a process called recombination, which causes the migrating electrons from the n-type to come in contact with the migrating holes from the p-type. A product of this process is charged ions, which result in an electric field.
3. Excited electrons: A difference in electric potential on a semiconducting material would cause it to leave thermal equilibrium and create a non-equilibrium situation. This introduces electrons and holes to the system, which interact via a process called ambipolar diffusion. Whenever thermal equilibrium is disturbed in a semiconducting material, the number of holes and electrons changes. Such disruptions can occur as a result of a temperature difference or photons, which can enter the system and create electrons and holes. The process that creates and annihilates electrons and holes are called generation and recombination.

In a semiconductor, current can be carried out by the flow of electrons or by the flow of positively charged holes in the electron structure of the material. Depending on this semiconductors are classified into two categories:

1. **Intrinsic Semiconductors**: An intrinsic semiconductor is made up of a very pure semiconductor material i.e. it is the one where the number of holes is equal to the number of electrons in the conduction band
2. **Extrinsic semiconductors:** Extrinsic semiconductors are those where a small amount of impurity has been added to the basic intrinsic material. The phenomenon of adding an impurity to the material is known as doping.

On the basis of this extrinsic semiconductors are of **two types**:

i. **P type semiconductor material:** In this type of semiconductor carries current predominantly as electron deficiencies called holes. A hole has a positive electric charge, equal and opposite to the charge on an electron. In a semiconductor material, the flow of holes occurs in a direction opposite to the flow of electrons. Add a trivalent impurity such as boron, aluminium, gallium etc to an intrinsic semiconductor creates deficiencies of valence electrons called holes.

ii. **N type semiconductor material:** In this type of semiconductor carries current

mainly in the form of negatively-charged electrons, in a manner similar to the conduction of current in a wire. Add pentavalent impurities such as antimony, phosphorus and arsenic contribute free electrons, greatly increasing the conductivity of the intrinsic semiconductor.

And, all semiconductor has a 2 kind while in the characteristic and precursor.

5.1. Organic semiconductor

The field of organic electronic is an active emerging technology with immense promise for innovative, convenient and high-performance electronics [147]. In the late 1970s three researchers found types of plastics capable of being modified to enable them as conducting metal. Conventional plastics are electrical insulators, but the discovery found they also can conduct electricity. It has opened a new era of plastics science and technology to be employed in organic semiconductors. Organic materials combine novel semiconducting electronic properties with the scope for easy shaping and manufacture of plastics. There is a nearly infinite variety of these organic materials and their properties can be tuned by changing their chemical structure, making them very versatile.

Because of the remarkable properties of these organic materials, they can be used to make a wide range of semiconducting electronic devices, such as transistors, light-emitting diodes, solar cells and even lasers. Organic semiconductor can provide us flat and flexible electronics, and light –emission from these materials is particularly promising- when a voltage is applied to a thin film of a semiconducting polymer to give out light. And it is possible to deposit semiconducting polymers to greatly simplify the manufacturing process, increase flexibility, and reduce cost. Organic semiconductors are proposed to provide potential solutions. Those advantages are resulted from the great characteristics of organic materials: easy shaping and manufacturing, infinite variety and tunable properties by changing the chemical structure.

5.1.1. Material

Organic materials are based on conjugated (class of carbon-based materials) organic small molecules and polymers. In the last decade, organic materials were used to produce plenty of products of devices, because they are large-area, low-cost, plastic substrates. Carbon-based materials have been widely used in the various applications such as batteries [148], [149], supercapacitors [150], [151], [152], fuel cells [153], [154] and photocatalysts [155], [156] due to their low cost and eco-friendliness. Since the successful isolation of 2D single layer of carbon atoms (viz. graphene) in 2004 by Geim and Novoselov [157], graphene has undoubtedly turned out to be one of the most important carbon-based materials due to its fascinating structural, optical and electronic properties [158], [159], [160].Compared with their widely known inorganic counterparts (mainly silicon, germanium, and metal oxide semiconductors), organic semiconductors offer some intrinsic advantages. Organic semiconductors offer several advantages because of their easy processing, good compatibility with a wide variety of substrates including flexible plastics and opportunities of modifying the structure of organic semiconductor. Also thin films of organic

semiconductors are mechanically robust and flexible and possible to get flexible electronics. The main advantage of organic semiconductor is assembled to a fully flexible insulating film without any substrate. Since the first report on the application of graphene in photocatalytic CO_2 reduction by Liang *et al.* [161], graphene has been often used in photocatalytic CO_2 reduction processes [162], [163]. Owing to its ultra-thin 2D layered structure, graphene features unique properties such as superior electronic conductivity, large specific surface area and high chemical stability, which are essential for enhancing photocatalytic CO_2 reduction performance. Therefore, graphene-based materials are the promising materials for photocatalytic CO_2 reduction.

5.1.2. Structure and properties

The structure of organic semiconductor devices is manufactured by an organic semiconductor uniform and high carrier transport property over a relatively large area. Modern chemistry enables the synthesis of complex molecules, such as carbon, hydrogen,

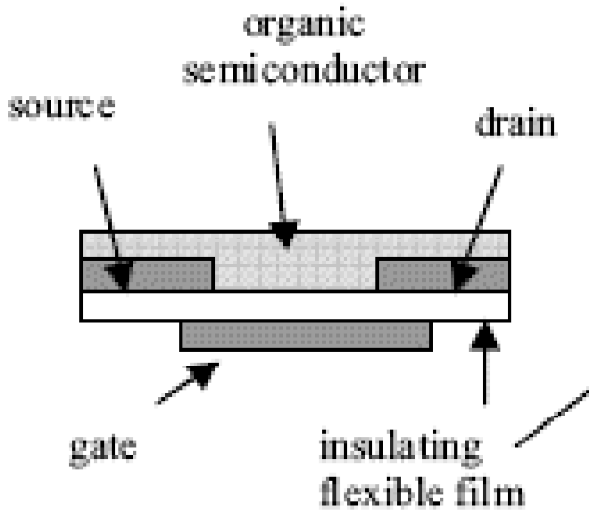

Figure 6: Structure of the Organic semiconductor transistor

oxygen, and nitrogen atoms. They can be linked together with strong covalent bonds where two neighboring atoms each as addiction. *F* or non-covalent interactions, they can be built to complex super molecular structures. They can approach nanotechnology; their interactions allow the materials to be tunable and mechanical properties. The structure of the Organic semiconductor transistor is shown in Fig. 6.

Carbon can form four bonds with neighboring carbon atoms or other atoms. Such as methane (CH4), four valence electrons occupy four sp3 in and can form four covalent bonds. When two adjacent carbon atoms come together, a band is formed between two electrons. The contribution of change has been observed in the crystal structure with

temperature to the variation of carrier mobility with temperature. With the temperature increasing, there will be slight increase in electron mobility along the crystal direction. Since the changes in crystal lattice dimensions of anthraquinone at various temperatures are small, the electronic band structure of organic compounds may be highly structure-sensitive.

5.1.3. Classification

Organic semiconductors can be widely classified into two groups on the basis of their molecular weight: conjugated polycyclic compounds of molecular weight less than 1000, and heterocyclic polymers with molecular weight greater than 1000. Due to the ease with which they form thin films with large surface area, polymers are very useful materials for semiconductors. Small-molecule organic semiconductors may further be classified as linear, two-dimensional fused ring compounds, and heterocyclic oligomers. It is more facile control of charge transport by modifying various molecular parameters. Organic semiconductors are an important class of functional materials. Numerous molecular and polymeric organic semiconductors have been developed for their great potentials in next generation flexible and printed electronics.

5.2. *Inorganic semiconductor*

Inorganic semiconductors, unlike their organic counterparts, are characterized by a relatively small exciton (e^--h^+) binding energy such that a distinction between the optical bandgap and electronic (or "transport") bandgap, is redundant. On the other hand, the

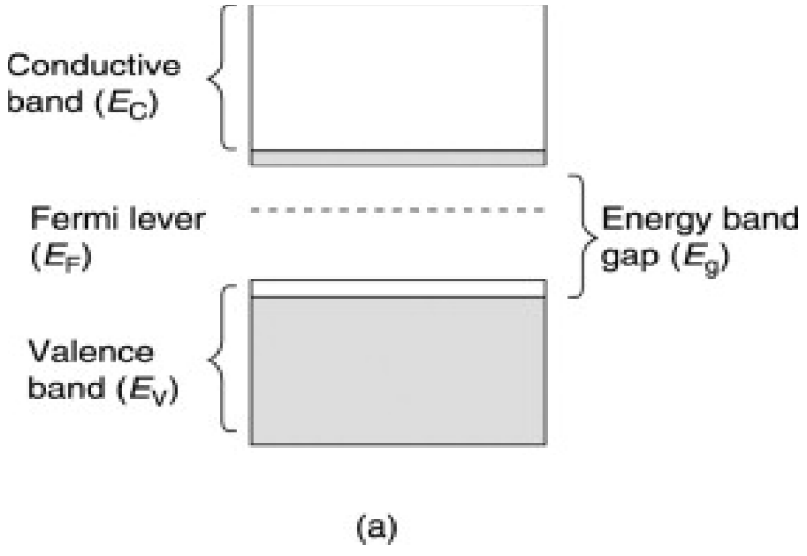

Figure 7: Energy band diagram of the inorganic semiconductor showing the valence band E_V, conduction band E_C, energy bandgap E_g, and Fermi energy E_F

distinction between direct vs. indirect bandgaps is very relevant to the present discussion. A semiconductor made from a noncarbon based material such as silicon, gallium or arsenide. Inorganic semiconductors are used in all logic and memory chips. In inorganic semiconductors charge transport can easily take place as a result of the strong covalent bonding between atoms in the lattice, which leads to a delocalization of the electronic states, Fig. 7. The fundamental difference between inorganic and organic semiconductors is in the charge transport mechanism. In the former case electrons moving in wide bands as delocalized plane waves are subjected to very limited scattering, and hence, feature relatively high mobility (e.g. ~1.5 $x10^3$ cm2V-1s-1 in Si at room temperature). In the case of organic semiconductors, the charge transport is based on carriers hopping between localized states associated with organic molecules. In the process electrons undergo significant scattering which results in very low electron mobility in organic semiconductors (~1-3 cm2V-1s-1). Both solids and both change their electrical properties once modified by doping or photo excitation. While **organic** semiconductors are "insulator-like" substances with typical band gap of 2.5–4 eV the **inorganic** have band gap of 1–2 eV and more similar to high resistance materials. Additional difference is in the building blocks. Organic are Carbon and Hydrogen based, pi bonded solids while inorganic are mostly coming from group 14 (pure) or from 13/15, 12/16 group (binary).

6. Bandgap

Band gap, in solid-state physics, a range of energy levels within a given crystal that are impossible for an electron to possess. In graphs of the electronic band structure of solids, the band gap generally refers to the energy difference (in electron volts) between the top

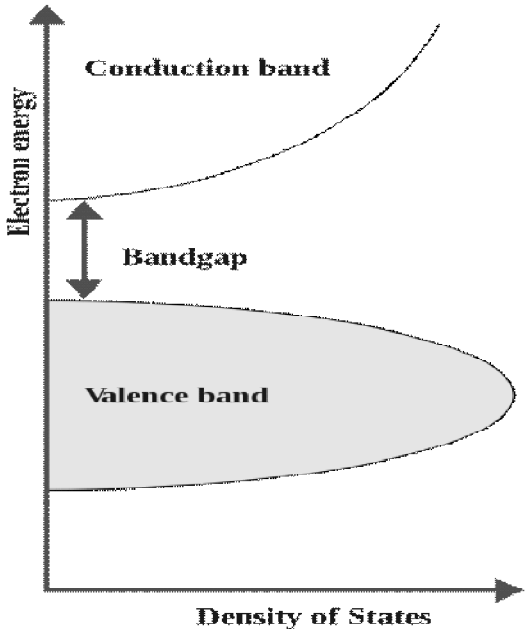

Figure 8: Semiconductor band structure

of the valence band and the bottom of the conduction band in insulators and semiconductors.

Valence band is completely full and the conduction band is completely empty, then electrons cannot move in the solid; however, if some electrons transfer from the valence to the conduction band, then current *can* flow (Fig. 8). Therefore, the band gap is a major factor determining the electrical conductivity of a solid. Substances with large band gaps are generally insulators, those with smaller band gaps are semiconductors, while conductors either have very small band gaps or none, because the valence and conduction bands overlap.

In semiconductor physics, the band gap of a semiconductor is of two types, a direct band gap or an indirect band gap. The minimal-energy state in the conduction band and the maximal-energy state in the valence band are each characterized by a certain crystal momentum (k-vector) in the Brillouin zone. If the valence band maximum and the conduction band minimum have the same crystal momentum (*k*-vector) in the Brillouin zone, then the resultant optical transition is termed a "direct" transition [164]. On the other hand, an indirect bandgap material would have to have phonon coupling for the optical transition to occur. For example, the 1.1 eV bandgap in single-crystal Si is indirect. It is indeed possible, for a given material, to possess both direct and indirect optical bandgaps [see below]. We note here that the nature of the transition (direct/indirect) (Fig. 9) has important implications on the photon-to-chemical conversion efficiency in both the PEC and PC scenarios, via dictating charge carrier lifetime and thus the recombination rate. Examples of direct bandgap material include some III-V materials such as InAs, GaAs. Indirect bandgap materials include Si, Ge. Some III-V materials are indirect bandgap as well, for example AlSb.

The optical energy bandgap, E_g, is a fundamental property of the inorganic semiconductor in a photo electrochemical (PEC) cell [165], [166], [167] for solar fuels generation. It dictates the amount of photon energy absorbed by the semiconductor from

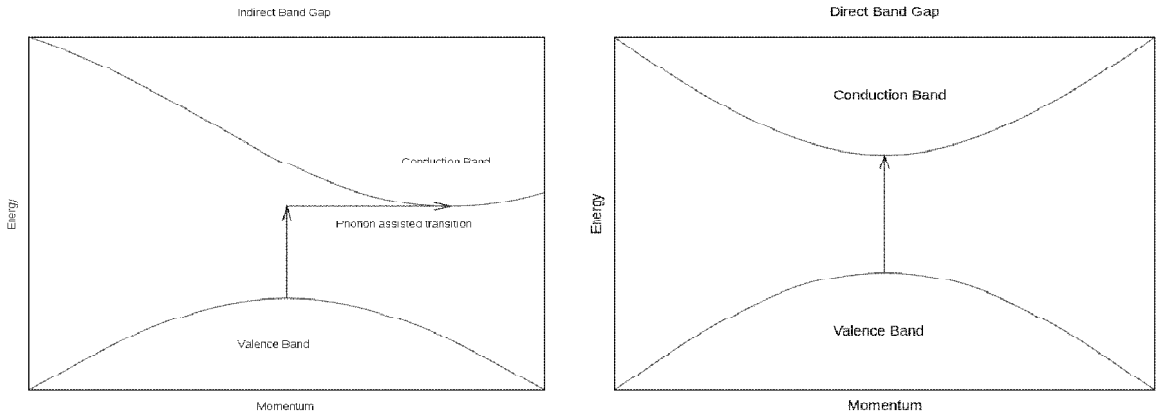

Figure 9: Indirect and direct bandgap

Table 1
Semiconductor

Catalyst types	*Composition*	*Excitation method*	*Application*
Semiconductor	Metal oxide, metal sulfide, metal nitride, metal-free semiconductors	Direct/indirect electron transition	Water splitting [140,141], CO_2 reduction [142], N_2 reduction [143,144], waste treatment [145]

Table 2
Characteristic of oxide semiconductor

Semiconductor	*Structure type*	*Optical bandgap (Eg) range (eV)a*	Comments
		Binary	
TiO_2	Anatase	3.0–3.5	Value depends on polymorph, ~0.2 eV higher for the anatase phase than for rutile.
ZnO	Wurtzite	3.2-3.4	-
WO_3	Monoclinic	2.5–2.9	-
Cu_2O	Cuprite	2.0–2.2	Very negative conduction band edge.
		Ternary	
$SrTiO_3$	Perovskite	3.2-3.8	Historically, one of the earliest ternary compounds studied for PEC applications.
$BiVO_4$	Scheelite	2.2–2.6	-
$Bi_2Ti_2O_7$	Pyrochlore	2.6–3.2	Other bismuth titanates also known; see Ref. [171].
$ZnFe_2O_4$	Spinel	1.7–4.8	-
$CuFe_2O_4$	Spinel	1.4–3.1	-
$PbMoO_4$	Wolfenite	1.7–4.1	-
$CuBi_2O_4$	Kusachite	1.4–1.8	-
$ZnNb_2O_6$	Columbite	3.6–4.1	-
$ZnWO_4$	Sanmartinite	3.1-4.4	-
$CuWO_4$	Wolframite	1.8?2.8	-

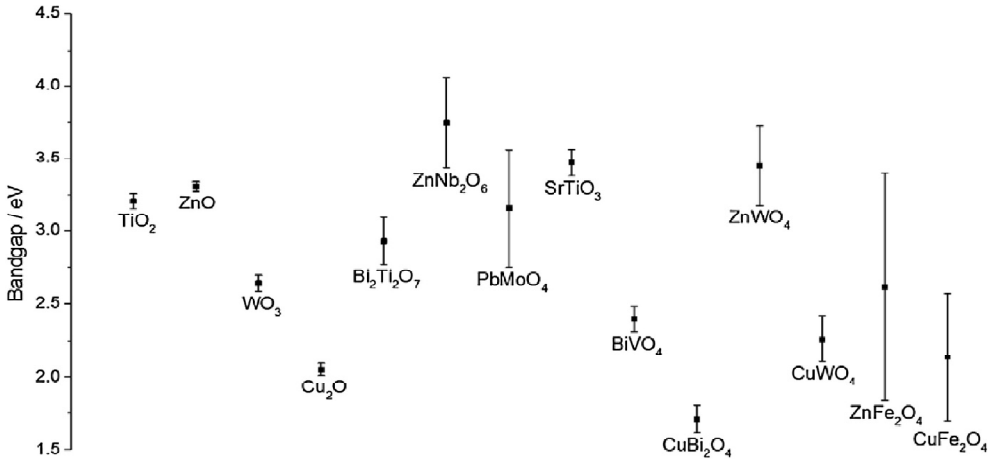

Figure 10: Variability of reported bandgap (E_g) values in the literature for the 14 oxide semiconductors

the excitation source (the Sun), and hence the ultimate photon-to-fuel conversion efficiency that can be achieved. During our ongoing, collaborative efforts to screen new generations of oxide semiconductor candidates for solar fuels generation [168], [169], [170], wide variations were noted in the reported bandgap values in the literature for a given semiconductor, especially for ternary oxides. Table 2 shows a bandgap energy (Fig. 10) and structure for some oxide semiconductors. Variation of bandgap energy might be attributed to alteration of electron energy level as well as phases present in each powder composition. For the undoped TiO_2 powder, the bandgap energy found in this study was 3.34 eV, which is in a comparable range of 3.20–3.40 eV, reported by numerous groups of research [172]. In general, the doping significantly affects bandgap energy of the materials. Ag doping results in an increase of electron density in structure at the energy lower than the conduction level of titanium dioxide (Table 3). With sufficient electron density, the electrons behave as the conduction band. Heterostructure of the titanium oxide and silver energy band results in the decrease of bandgap energy. In addition, the titanium dioxide with 2.5 and 5 mol% Ag, the rutile phase was also evident. With the bandgap energy close to 3.0 eV, the presence of rutile might contribute to further decrease of bandgap energy of the powders. At Ag doping of 10 mol%, partial filling of conduction band might occur. This could attribute to a blocking of the lowest energy state, which consequently result in an increase of bandgap energy [173].

Table 3
Bandgap energy of the synthesized titanium dioxide powders including a different concentration of Ag

Ag content (mol%)	*Bandgap energy (eV)*
0	3.34
2.5	3.11
5	3.04
10	3.28

7. Photocatalyst

Semiconductor photocatalysis has been regarded as one of promising approach to solve the environmental pollution and energy crisis. Semiconductor based photocatalysis is one of the most promising technologies to solve the energy and environmental crisis [[174], [175], [176]]. A number of photocatalysts were synthesized and used for light induced chemical transformations, such as ZnO [177], TiO_2 [178], CdS [179], and g-C_3N_4 [[180]. Photocatalysts could be roughly separated into 2 categories. One is semiconductor photocatalyst. It contains metal oxides, nitrides or sulfides, such as TiO_2[181] and MoS_2[182], and the metal-free semiconductor such as C_3N_4. The other is the metal nanoparticles that possess localized surface plasmon resonance (LSPR) property. Copper, gold and silver nanoparticles are widely reported to exhibit strong LSPR effect under visible light irradiation. The general mechanism of redox reaction with semiconductors as photocatalysts is shown in Fig. 11. It consists of the following 3 consecutive steps. Firstly, the electron in the valence band of the semiconductor is excited and jumps into its conduction band with light assistance. Subsequently, the excited electrons and holes are transferred to the surface of the catalyst.

Then the electron is consumed in the reduction reaction, while the hole, which carries the positive charge, is used in the oxidation reaction.

7.1. Metal semiconductor photocatalyst

Since the application of n-type TiO_2 in water splitting as a photoelectrocatalyst in 1972, more than 130 inorganic materials, including metal oxides, nitrides or sulfides, have been tested [183] and approved to be promising as photocatalysts. Most effective metal oxide semiconductors in photocatalytic reactions are consisted of d^0 or d^{10}elements such as Ti, V, Zr, Ga, Ge, etc. The conduction bands of these metal oxides are usually consisted of the d (for d_0 elements) or sp orbitals (for d_{10} elements) while the valence band is provided by the 2p orbitals from oxygen atoms. As for the metal nitride or sulfide, the valence band is provided by the 2p orbitals from nitrogen or the 3p orbitals from sulphur atoms. In some specific examples, the valence band may also be provided by the 3d orbitals from Cu [184], 4d orbitals from Ag [185], 6s orbitals from Pb or Bi [186], or 5s orbitals from Sn [187]. Metal semiconductor photocatalysts have been widely used in photocatalytic area. One of the most notable examples is the photocatalytic water splitting reaction over TiO_2 which has been conducted since the 70s of the last century. Nowadays, the metal semiconductors have also been applied in some other photocatalytic reactions. For example, Xu *et al.* employed $CsPbBr_3$ and carbon dots in carbon dioxide photoreduction [188]. Chen and co-workers raised a highly effective photocatalyst based on ZnO for organic pollutant photo-degradation [189].

7.2. Metal-free semiconductor photocatalyst

Metal semiconductors granted a great success in photocatalysis, and have been applied in versatile photocatalytic reactions such as water splitting, ammonia synthesis and carbon dioxide reduction [190], [191] . However, some of the metal semiconductors suffer from the following three shortages. Some of them are consisted of, or combined with, noble metals, such as Pt [192], Au [193], Pd [194], etc, when used as photocatalysts. The high prices of these noble metals increase catalyst costs and limit their applications in industrial scale. The heavy metals which are used in these semiconductor photocatalysts may be released into the environment through photo-corrosion . Consequently, a proper disposal of the reaction waste should be taken into account. Some metal semiconductor photocatalysts, such as TiO_2 and ZrO_2, have relatively large band gaps, which prohibit the utilization of the abundant visible light. The electrons in rutile TiO_2 can only be stimulated by UV light since the energy of visible light is not strong enough to stimulate the electron/hole separation over TiO_2. In fact, only less than 5% of solar light allocates in UV light region, leading to that most metal semiconductors cannot harness the solar light effectively [195]. To deal with the problems that exist on the metal oxide semiconductor photocatalysts, metal-free semiconductors have drawn a huge amount of attention of scientist. One representative example of metal-free semiconductors is graphitic carbon nitride (g-C_3N_4), which was firstly synthesized in 1834 . The band gap of g-C_3N_4 is 2.7/ eV, less than 3.2/ eV, which is the upper limitation for semiconductors in absorbing visible light [196].

8. Mechanisms of enhancement of photocatalysis by Graphene

Graphene and semiconductor materials have been used together in photocatalysts for a relatively short period, and the mechanisms resulting in enhanced photocatalysis by these composite photocatalysts are currently largely unclear. To date, numerous reports have concluded that the mechanisms of enhanced photocatalysis are as follows. Collection and transport of excited electrons from semiconductors: semiconductors usually possess a low energy valence band (VB) that is full of electrons, a high energy conduction band (CB) with empty orbitals and band gap between them. When a semiconductor is irradiated by light of energy equal to or stronger than the band gap energy (Eg), electrons in the VB are excited and transited to the CB, which produces corresponding holes in the VB and electron hole pairs. The electrons and holes, which have lifetimes of nanoseconds, are either transferred to the surface where they take part in redox reactions or recombine to reform the ground state. When GR is introduced into a photocatalytic system, because the CB of most of semiconductors is higher than the Fermi level of GR, the photogenerated electrons are readily transferred from the semiconductor to GR by passing through the interface between them. When the CB of a semiconductor is lower than the Fermi level of GR, the photogenerated electrons cannot be transferred from the semiconductor to GR. If there are sensitizers in the system, they will be sensitized by absorbing photons to generate electrons. Because the Fermi level of GR is higher than the CB of semiconductors, electrons are transferred from sensitizers to GR and then to the semiconductor. Because of the extremely high conductivity and unique two dimensional planar structure of GR, it can increase the rate of transfer of photo generated charge carriers from GR to semiconductors and then to the surfaces of reactants. This increases the mean free path of electrons, and reduces the recombination of photogenerated electrons and holes, which enhances the photocatalytic quantum efficiency of semiconductor/GR composites [197–199]. The band structure diagram of GR and some common semiconductors, and the major routes of GR to enhance photocatalysis, are displayed in Fig. 12(a) and (b), respectively. This mechanism has been deduced by comparing the results of most reported photocatalytic reaction.

9. Fundamentals of reduction

Photocatalysts can be categorized based on their structure or chemical nature. Three categories as described by Nikokavoura & Trapalis are (1) Inorganic: single-metal oxides, mixed-metal oxides, metal oxide composites, layered double hydroxides(LDH) and salt composites, (2) carbonaceous: graphene (GR), carbon nanotubes(CNTs) and g-C_3N_4 composites and (3) hybrid organic-inorganic photocatalytic materials. Each of the category's irradiation and experimental conditions requirement as reported are listed in Table 4. CO2 is a kinetically and thermodynamically stable molecule, thus CO2 conversion reactions are endothermic and need efficient catalysts to obtain high yield.

The **electrochemical reduction of carbon dioxide** (**ERC**) is the conversion of carbon dioxide to more reduced chemical species using electrical energy. The first examples of electrochemical reduction of carbon dioxide are from the 19th century, when carbon dioxide

Table 4
Photocatalyst categories for carbon dioxide reduction, irradiation type and experimental medium

Description	*Irradiation type*	*Experimental conditions*	*Example*
		Inorganic	
Single-metal oxides	UV/Vis	Solid-gas (catalyst-CO_2/H_2O, catalyst-CO_2/H_2, catalyst-CO_2/CH_4) systems/Aqueous dispersions	TiO_2, WO_3, ZnO, Pb_3O_4, BiOI, CeO_2
Mixed metal oxides	UV/Vis	Solid-gas (catalyst- CO_2/H_2O) systems/Aqueous dispersions	$BiVO_4$, Bi_2WO_6, $CaFe_2O_4$, $LaCoO_3$, $NaBiO_3$, $NaNbO_3$, $KNbO_3$, $CuGaO_2$, $CuAlGaO_4$
Metal oxide composites	Vis	Solid-gas (catalyst- CO_2/H_2O) systems/Aqueous dispersions	NiO/$InTaO_4$ Pt (0.5%wt)/$ZnAl_2O_4$/ZnGaNO, CuO/ZnO supported on MgO
Layer Double Hydroxides (LDHs)	UV/Vis	Solid-gas (catalyst- CO_2/H_2O, catalyst- CO_2/H_2) systems/ Aqueous dispersions	Zn-Cu-Ga layered double hydroxide (LDH)
Salt composites	UV/Vis	Aqueous/organic solutions	CdS on 2-propanol, thiol modified CdS in DCM
		Carbonaceous	
Graphene (GR) based	Vis	Aqueous dispersions	$(BiO)_2CO_3$/GR
Carbon nanotubes (CNTs) based	Vis	Aqueous dispersions	Ag/AgBr/CNT
g-C_3N_4 based	Vis	Aqueous dispersions/Solid-gas (catalyst- CO_2/H_2O) systems	WO_3/g-C_3N_4 composites
Hybrid organic-inorganic	Vis	Aqueous/organic solutions	Zeolitic imidazolate frameworks (ZIFs)

was reduced to carbon monoxide using a zinc cathode. Research in this field intensified in the 1980s following the oil embargoes of the 1970s. Electrochemical reduction of carbon dioxide represents a possible means of producing chemicals or fuels, converting carbon dioxide (CO_2) to organic feed stocks such as formic acid (HCOOH), methanol (CH_3OH), ethylene (C_2H_4), methane (CH_4), and carbon monoxide (CO).

Photochemical carbon dioxide reduction harnesses solar energy to convert CO_2 into higher-energy products. In decades, the utilization of solar energy via photocatalytic or photoelectrocatalytic (PEC) CO_2 reduction to organic compounds is always a big challenge for scientists who work on the chemistry, materials and environment science [200], [201]. Nowadays, number of investigations have focused on the photocatalytic reduction [202], [203], or electrocatalytic reduction of CO_2 using semiconductors as catalysts, including the n-type semiconductors of TiO_2 [204], ZnO, ZnS [205], CdS [206] and p-type semiconductors of Cu_2O [207], GaN, GaP [208], NiO [209], Co_3O_4 [210], SiC [211] etc.

In which, TiO_2 is widely employed in the CO_2 reduction [212]. Although TiO_2 has many advantages such as non-toxicity, cost inexpensive, physical and chemical stability [213], its low electron mobility limits the separation of electrons and holes and the efficiency of CO_2 reduction. Among various semiconductors for CO_2 reduction, the ZnO is emerging as an alternative n-type semiconductor that was used as well in CO_2 reduction in our previous report and other literature [214].

9.1. Photo electrochemical reduction

Mimicking nature's photosynthesis process, photoreduction of CO_2 is one of the most alluring methods for CO_2 conversion due to the abundance and free access of sunlight. To meet with global energy demands, Lewis and Nocera have proposed to convert and store solar energy in chemicals (H_2, methanol, and hydrocarbons) via the photosynthetic process [215]. Solar radiation varies across the globe from altitude, height, atmospheric conditions, and season. For example, solar radiation for flat-plates facing south at a fixed tilt in New York City is about 2–6 kWh/m_2/day. A typical photoreduction electrode is composed of a semiconductor and photocatalysts, and many of these are transition metal complexes. Semiconductors absorb photons to make excited electrons transfer from a valence band to the conducting band, which is then transferred to a photocatalyst complex, which reduces CO_2 to CO and other useful organic compounds. Such photoelectrocatalytic processes should be distinguished from purely photocatalytic routes. Kubiak and Kumar reported the photo-assisted electrochemical reduction of CO_2 to CO on Re(bipy-But)(CO)3Cl((bipy-But) = 4,40-ditert- butyl-2,2-bipyridine)/p-type silicon with a Faradaic efficiency of 973%, and a short-circuit quantum efficiency of 61% for light-to chemical energy conversion, and an overall efficiency of about 10% for the conversion of polychromatic light [216]. Smieja *et al.* further reported that the electron transfer from the electrode to the catalyst can be controlled by modifying the p-Si surface with phenyl ethyl groups. The interaction experiments of the electrocatalyst with the targeted catalytic substrate CO_2, H_2O, and CH_3OH show that the reaction with CO_2 is about 25 times faster than that with H_2O, and 50 times faster than that with CH_3OH. Calculations based on density functional theory (DFT) show that the nature of the binding of CO_2 to the anion forms a Re (bipy-tBu)(CO)3(CO_2)K complex [217]. Kaneco has developed metal-modified p-InP hotoelectrodes for the photo electrochemical reduction of CO_2 in the LiOH/ methanol-based electrolyte. Ag, Au, Pd, and Cu deposited p-InP photo electrodes show higher selectivity to CO than that to H_2. Ag deposited p-InP photo electrode show maximum current efficiency of carbon monoxide (rf = 80.4%) and Pd deposited p- InP photo electrode has the highest selectivity to CO (100%) [218]. BoHan JixianWang ChaoxianYan YapengDong YanjieXu RongNie HuanwangJing has research in The photoelectrocatalytic CO_2 reduction on TiO_2@ZnO heterojunction by tuning the conduction band potential. Figure 13 shows a morphology structure of TiO_2@ZnO.

In this photo electrocatalysis experiments were performed in a closed self-designed quartz reactor equipped with a working photocathode of M-TiO_2@ZnO/FTO and a counter electrode of $BiVO_4$ and powered by an external Si-solar cell (–0.6 < –1.0/ V).

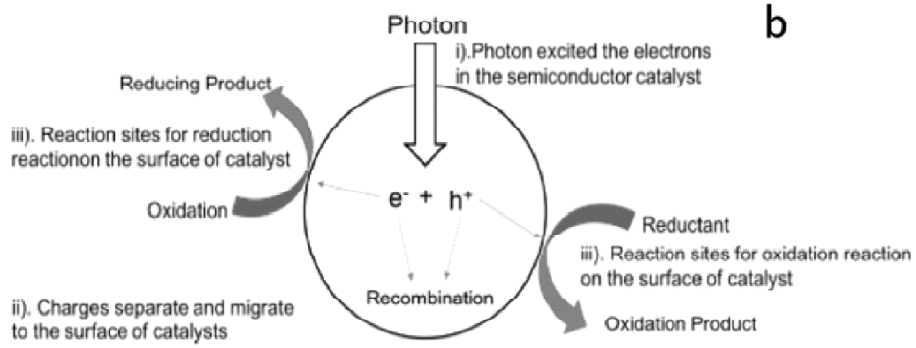

Figure 11: Mechanism of photocatalysis reactions driven by a semiconductor

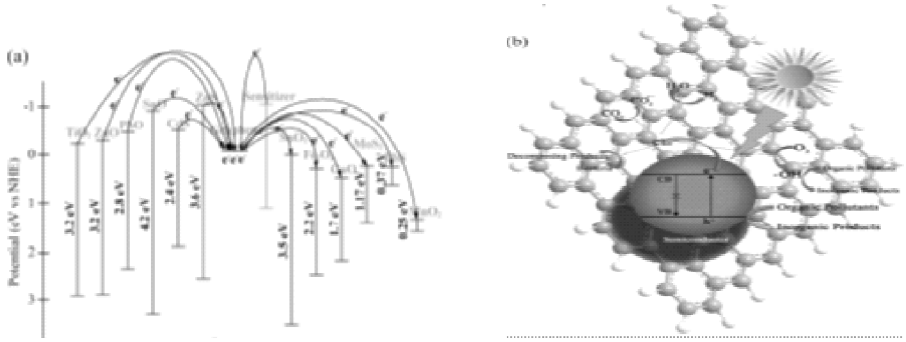

Figure 12: Photocatalytic mechanisms of semiconductor/GR composites . (a) Band structure diagram of GR and common semiconductors; (b) Major routes of enhanced photocatalysis by GR including improved charge collection and transfer

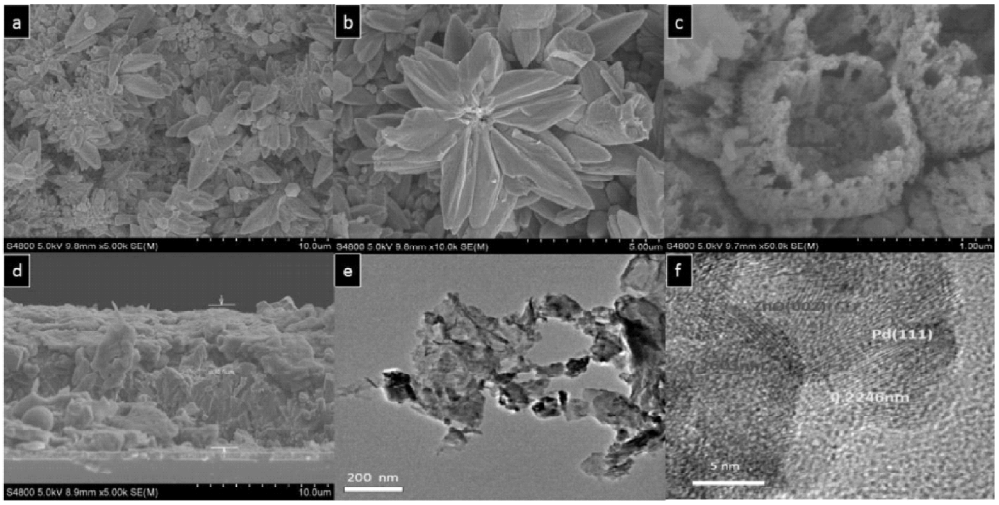

Figure 13: (a, b) SEM image of ZnO/FTO surface morphology; (c) SEM image of Pd-TiO_2@ZnO/FTO surface morphology; (d) cross-sectional of Pd-TiO_2@ZnO/FTO SEM image; (e) bright-field TEM image and (f) corresponding HRTEM image of Pd-TiO_2@ZnO/FTO.

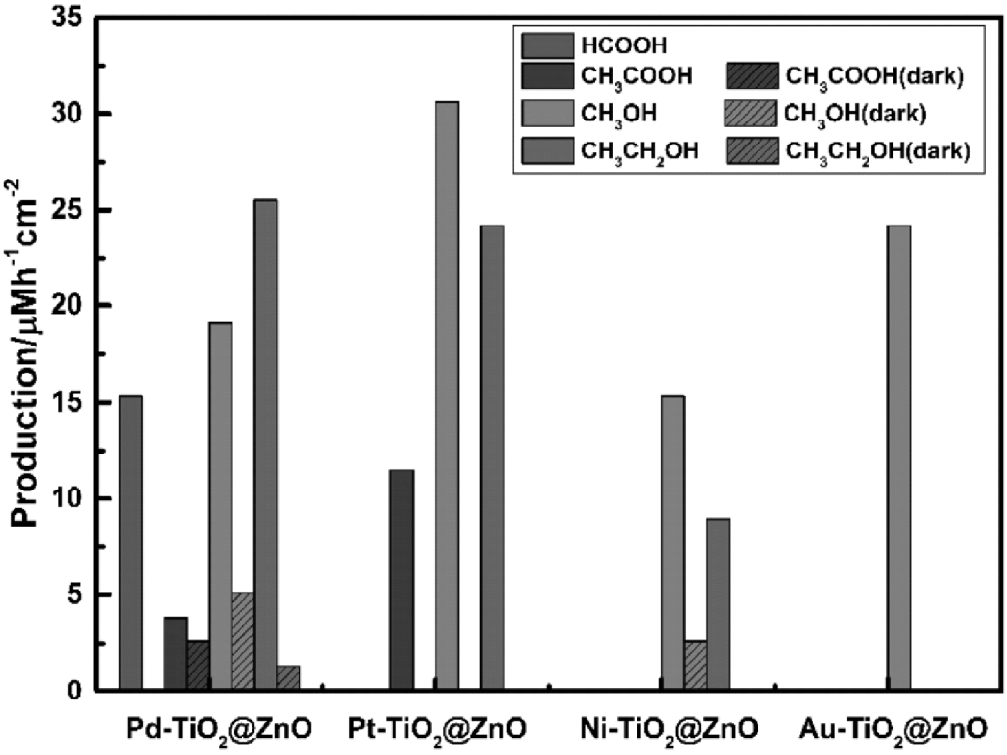

Figure 14: The formation rates of liquid products for various dye/M-TiO_2@ZnO/FTO photo cathodes at –1.0 voltage.

The electrolyte was CO_2 bubbled aqueous solution of $KHCO_3$ (0.1 M, 60 mL), in which, dye Eosin Y was added as a photosensitizer (1 mM). Subsequently, the photo electrocatalysis cell was irradiated by a 300 W Xenon lamp under light density of 200 $mWcm^2$. The control experiment of CO_2 reduction was conducted as well without irradiation of Xenon lamp. Photo electrocatalytic reduction of CO_2 with fabricated photocathodes of M-TiO_2@ZnO/FTO has been carried out. The results were illustrated in 14. Fig. 14, different metal deposition shows various selectivity to hydrocarbons. It is worth to mention that the Pd-TiO_2@ZnO/FTO and Ni-TiO_2@ZnO/FTO electrodes can produce hydrocarbons even under dark conduction. Only trace of H_2 and O_2 gases can be examined in the cell of dye/Pd-TiO_2@ZnO/FTO||$BiVO_4$. The formation rate of liquid products is about 62.4 μmol/ cm^{-2}/ h^{-1}, which is two times than our results of semiconductors [219] and 100-fold higher than the literature result (0.6 μmol/ cm^{-2}/ h^{-1}) [220]. After that, the CB bands of ZnO/FTO, TiO_2@ZnO/FTO, Pd-TiO_2@ZnO/FTO, Pt-TiO_2@ZnO/FTO, Ni-TiO_2@ZnO/FTO and Au-TiO_2@ZnO/FTO were estimated and depicted in Fig. 15. The CB potential of heterojunction TiO_2@ZnO/FTO in the working electrolyte is –0.15 V that is slightly higher than that of ZnO/FTO (–0.13 V). These CB potentials lowering than pure semiconductors are attributed to the contribution of SnO_2

(–0.1 V) on the FTO substrate. On the contrary, the metal deposition would augment the CB band level of heterojunction electrodes of M-TiO_2@ZnO/FTO that were in agreement with our previous reports [221].TiO_2@ZnO/FTO were obviously enhanced to –0.39 and –0.26/ V, respectively. The Pt and Au metal particles could slightly enhance the CB bands of heterojunctions of Pt-TiO_2@ZnO/FTO and Au-TiO_2@ZnO/FTO to –0.19 and –0.18 V, respectively. Generally, the CB potentials of electrodes must be more negative than the standard reduction potential of products [222]. Figure 16 shows a mechanism of M-TiO_2@ZnO/FTO in CO_2 reduction.

9.2. Photocatalytic CO_2 reduction

Photocatalytic CO_2 reduction over carbon-based 2D layered materials for the production of solar fuels. In particular, the photocatalytic CO_2 reduction process involves a series of reactions including: (1) CO_2 adsorption, (2) electron–hole pair photo generation, (3) charge carriers separation, (4) charge carriers transportation, and (5) chemical reactions between surface species and charge carriers [223]. The photocatalytic CO_2 process starts with adsorption of CO_2 molecule on the photocatalyst surface. Lixin Zhang, Changhui Ni, Hongfang Jiu, Chunmei Xie had research in photocatalytic carbon dioxide reduction with graphene based nanocomposite. In this research, using a one-pot synthesis with prepare a nanomaterials and this nanocomposite including a TiO_2 semicondutor. This semiconductor is strong oxidizing power, nontoxicity, high chemical stability, and photostability, TiO_2 has been widely used and studied as photocatalyst [224–226]. However, the band gap of TiO_2 is 3.2 eV, which could only absorb the ultraviolet region of the sunlight. In addition to this, noble metal (Ag or Au) doping is an effectively method to improve photocatalytic performance [227]. Several research works focusing on Ag-TiO_2/graphene nanocomposite. Vasilaki E *et al.* prepared Ag-loaded TiO_2/reduced graphene oxide by a two step method. The structure and morphologies of prepared samples were characterized by TEM and HRTEM shown in Fig. 17. Fig. 17a, the r-GO

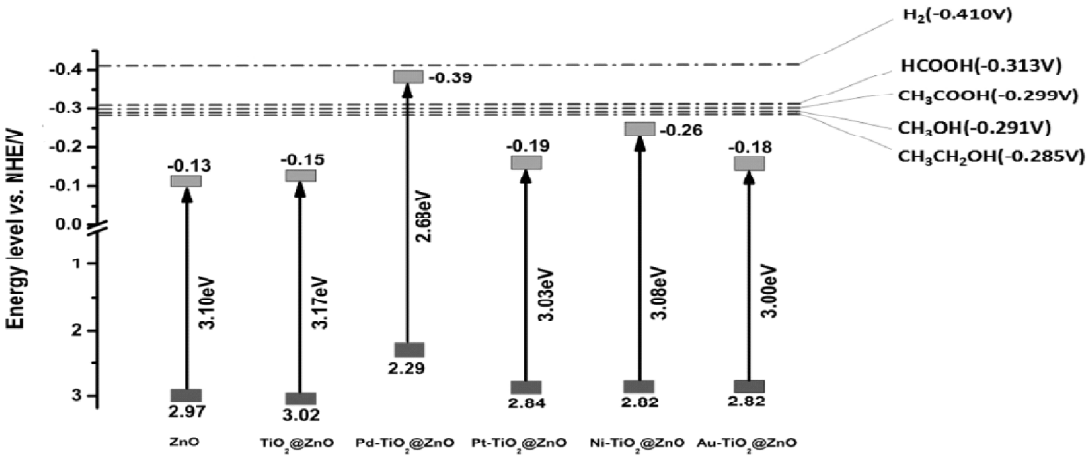

Figure 15:Schematic diagram of CB and VB for photocathodes.

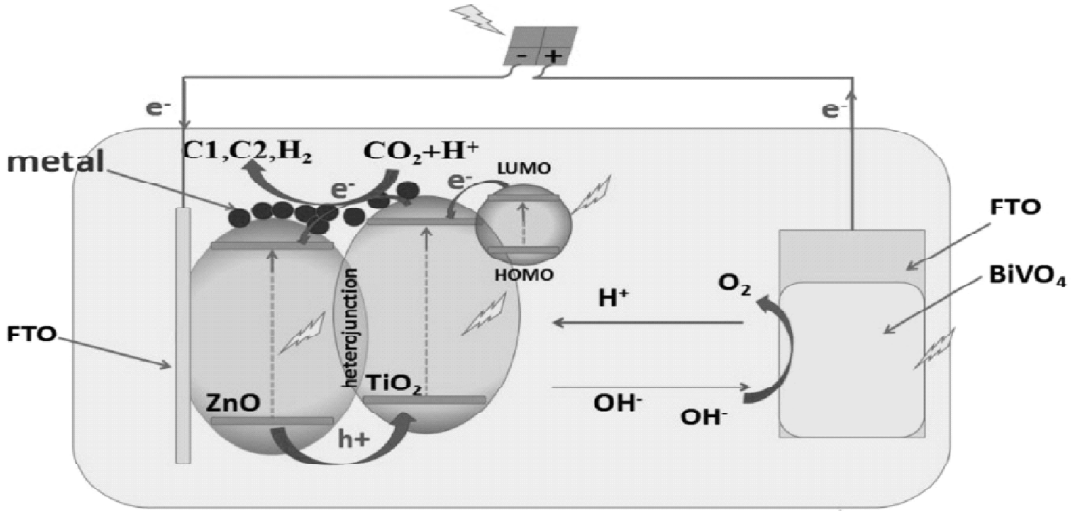

Figure 16: Schematic mechanism for CO_2 reduction to hydrocarbons in the PEC cell of dye/M-TiO_2@ZnO/FTO|$KHCO_3$|$BiVO_4$.

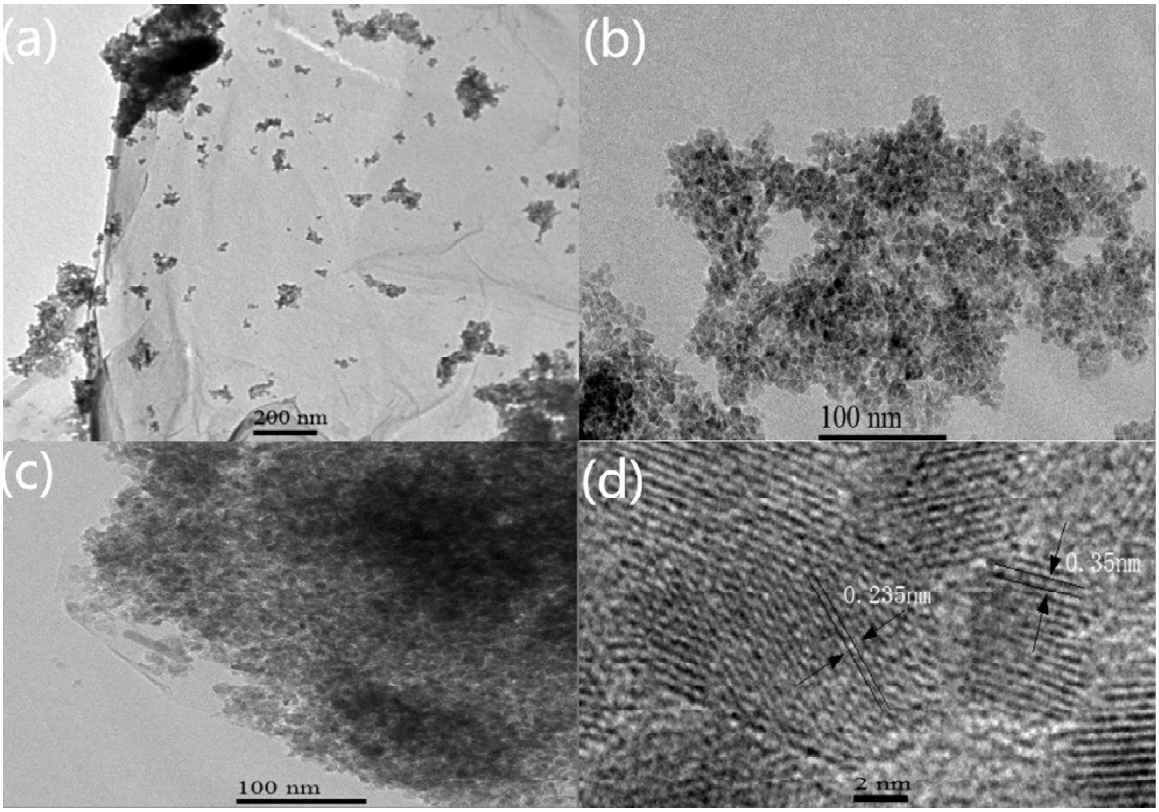

Figure 17: TEM(a) and HRTM(b, c, d) of prepared Ag-TiO2/reduced graphene oxide nanocomposite

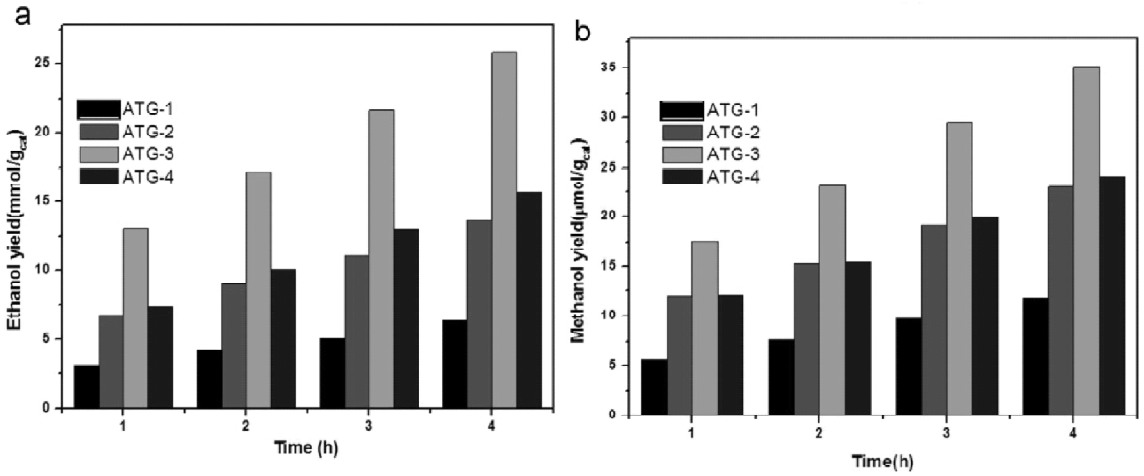

Figure 18: The yield of main liquid product under visible light irradiation

Table 5
TiO_2 base photocatalytic CO_2 reduction system

Photocatalyst	*Reductant*	*Methodology*	*Process Condition*	*Yield*	*Reference*
Bi2S3 QD/TiO_2(001) facets	Iso-propanol	Solvothermal synthesis	Quartz reactor, catalyst 12?mg, 250 Hg lamp	CH3OH 1169.15 μmol/ g.h	[228]
Cu/TiO_2	H_2O	Hydrothermal	Quartz tube reactor, photocatalyst 40mg, 100 W Hg lamp λ <390 nm, 150°C,	CO / 7.5μmol/ $g_{catalyst.}$h	[229]
Ag/TiO_2	H_2O	Sol-gel technique	Fixed bed reactor, photocatalyst 0.1g, UV light 254 &365 nm, 25 °C, 1 atm	CH4 / 10.5 CH3OH / 2μmol/ $g_{catalyst}$	[230]
TiO_2	H_2O	Commercial	High Pressure photoreactor, Photocatalyst 0.5g/L, 7 bar, 80 °C,	H2/HCHO/ HCOOH 102/16537/ 2954.3 mmol/ Kg.h	[231]
Cu/TiO2-SiO2	H_2O	One-pot sol-gel method,	Stainless steel reactor, UV light (250 nm <λ <400 nm), 25 °C, 1 atm	CO / 60 CH4 / 10 μmol/g catalyst.h	[232]
Au/TiO2	H_2O	Deposition-precipitation method	Steel reactor, photocatalyst 0.1g, 6 W lamp, CO2/H2O:7.25, 2 bar, 50 °C	CH4 / 8.0 μmol/gcataly st.h	[233]

Photocatalyst	*Reductant*	*Methodology*	*Process Condition*	*Yield*	*Reference*
CuO/TiO_2	H_2O	Sol-gel & Impregnation	Double wall cylindrical reactor, 6 W Mercury lamp, Photocatalyst 0.1 g	CH3OH 4120μmol/ g	[234]
Carbon@ TiO_2	H_2O	Hydrothermal and hydrolysis	Pyrex glass reactor, 300W Xe lamp, Photocatalyst 0.1g	CH4/CH3OH 4.2/9.1 μmol/g.h	[235]
La/TiO_2	CH4	Sol-gel method	Stainless steel cylindrical vessel, Photocatalyst 25mg, 200W Xe lamp,	C2H6 / 492.8μmol/ g	[236]
Fluorinated TiO_2-SiO_2	H_2O	Evaporation & solvo-thermal process	Homemade reactor, photocatalyst 0.2 g, 300 W Xe lamp	CH4 /2.42 μmol/g, catalyst	[237]
TiO_2 (001) TiO_2 (101)	H_2O	Solvothermal method	Fixed bed reactor, photocatalyst 100mg, 300W Xe lamp, UV light, 25 °C, 1 atm	CH_4 / 1.35 μmol/g, catalyst.h	[238]

possesses a 2D layered structure with many wrinkles at the edge. Fig 17b, Ag-TiO_2 nanoparticles distributed on the surface of r-GO. Fig. 17d can be attributed to the d-spacing value of the Ag (111) plane and the anatase (101) plane of TiO_2.

The photocatalytic ability of prepared samples was also evaluated by the reduction of CO_2. The concentration of main liquid products (Methanol and Ethanol) was analyzed by a gas chromatograph. There was no obvious peak on GC for pure TiO_2 after 4 h visible light irradiation, which demonstrated that the pure TiO_2 don't possess photocatalytic ability under visible light irradiation. It accords with above result well. The yield of main liquid products was shown in Fig. 18.

And finally, several modifications such as metal and non-metal doping, co-photocatalyst, semiconductor coupling, crystal and facet engineering, state of the art morphologies and novel structures have been applied to boost the efficiency of TiO_2-based photocatalytic systems. Herein, promising strategies to enhance the various aspects of TiO_2-based CO_2 reduction system such visible light response, charge carrier's separation, CO_2 adsorption, and state of art morphologies of photocatalyst have been elaborated.

10. Conclusions and outlook

Fundamental aspects of photocatalytic CO_2 reduction like thermodynamics, mass transfer, selectivity and reaction mechanism have been deliberated. Strategies to improve

the efficiency by modifying the various aspects of TiO_2-based photocatalytic system have been discussed in detail. Overall, it can be concluded that modified TiO_2 nanocomposites are efficient for CO_2 reduction to produce solar fuels. The yield and efficiency of process have been significantly refined by recent efforts particularly through multinary and functionalized photocatalysts. The VLR, charge recombination and CO_2 adsorption problems have been largely improved by recently fabricated composites with unique morphology and large exposed active sites. Moreover, addition of graphene to photocatalysts have revamped the efficiency and improved the yield. Nevertheless, basal plane defects limit the electronic conductivity of graphene, photocatalytic performance can further be amplified by defects free graphene as bridge in multinary nanocomposites. Although, significant advancements have been made in theoretical basis and performance of TiO_2-based photocatalytic CO_2 reduction system, it is still far away from practical applications. Currently, most of visible light active TiO_2 composites are dyes or sulfides coated, and they suffer from photocorrosion problem. Visible light active stable nanocomposites are essential for efficient solar fuel production. Dyes must be replaced by low bandgap energy semiconductors, quantum dots, and novel photonic crystals where band gap and propagation of light can be tuned to any desire wavelength of light. Furthermore, narrow bandgap semiconductors should be used to simultaneously achieve high visible light activity as well as charge separation. The challenge of selectivity of singular product could also be resolved by discovering the CO_2 reduction mechanism. Last, thermodynamic aspects should be investigated in detail to dig out the mechanism of photogenerated electrons and CO_2 reduction reaction. Finally, photocatalytic CO_2 reduction is still at embryonic stages and current progress is far from practical applications. Therefore, there is a need of tremendous efforts to explore the causes of the low efficiency and yield. Hence, theoretical knowledge gaps and experimental impediments must be overcome to transform CO_2 into solar fuels at large scale.

Acknowledgement

This research was supported by the Basic Science Research Program through the National Research Foundation of Korea (NRF) funded by the Ministry of Science, ICT and future Planning (2018R1D1A1A09082321).

Reference

[1] EIA-International Energy Outlook 2017. https://www.eia.gov/outlooks/ieo/. November 15, 2017.

[2] L. Gustavsson, S. Haus, M. Lundblad. Climate change effects of forestry and substitution of carbon-intensive materials and fossil fuels. Renew. Sustain Energy Rev., 67 (2017), pp. 612-624.

[3] M. Höök, X. Tang. Depletion of fossil fuels and anthropogenic climate change—a review. Energy Policy, 52 (2013), pp. 797-809.

[4] J. Santos, A. Cesarin, C. Sales, M. Triano. Increase of atmosphere $_CO_2$ concentration and its effects on culture/weed interaction. World Acad., 11 (2017), pp. 371-378.

[5] T. Covert, M. Greenstone. Will we ever stop using fossil fuels?. J. Econ. Perspect., 30 (2016), pp. 117-138.

[6] J.G. Yu, J.X. Low, W. Xiao, P. Zhou, M. Jaroniec. Enhanced photocatalytic CO_2-reduction activity of

anatase TiO_2 by coexposed {001} and {101} facets. J. Am. Chem. Soc., 136 (2014), pp. 8839-8842.

[7] D. Chen, X. Zhang, A.F. Lee. Synthetic strategies to nanostructured photocatalysts for CO_2 reduction to solar fuels and chemicals. J. Mater. Chem. A, 3 (2015), pp. 14487-14516.

[8] Q.J. Xiang, B. Cheng, J.G. Yu. Graphene-based photocatalysts for solar-fuel generation. Angew. Chem. Int. Ed., 54 (2015), pp. 11350-11366.

[9] E.V. Kondratenko, G. Mul, J. Baltrusaitis, G.O. Larrazábal, J. Pérez-RamírezStatus and perspectives of CO_2 conversion into fuels and chemicals by catalytic, photocatalytic and electrocatalytic processes. Energy Environ. Sci., 6 (2013), pp. 3112-3135.

[10] L. Yuan, Y.J. Xu. Photocatalytic conversion of CO_2 into value-added and renewable fuels. Appl. Surf. Sci., 342 (2015), pp. 154-167.

[11] T. Inoue, A. Fujishima, S. Konishi, K. Honda. Photoelectrocatalytic reduction of carbon dioxide in aqueous suspensions of semiconductor powders. Nature, 277 (1979), pp. 637-638.

[12] M. Marszewski, S.W. Cao, J.G. Yu, M. Jaroniec. Semiconductor-based photocatalytic CO_2 conversion. Mater. Horiz., 2 (2015), pp. 261-278.

[13] X. Li, J.Q. Wen, J.X. Low, Y.P. Fang, J.G. Yu. Design and fabrication of semiconductor photocatalyst for photocatalytic reduction of CO_2 to solar fuel. Sci. China Mater., 57 (2014), pp. 70-100.

[14] A.J. Morris, G.J. Meyer, E. Fujita. Molecular approaches to the photocatalytic reduction of carbon dioxide for solar fuels. Acc. Chem. Res., 42 (2009), pp. 1983-1994.

[15] S.C. Roy, O.K. Varghese, M. Paulose, C.A. Grimes. Toward solar fuels: photocatalytic conversion of carbon dioxide to hydrocarbons. ACS Nano, 4 (2010), pp. 1259-1278.

[16] S.N. Habisreutinger, L. Schmidt-Mende, J.K. Stolarczyk. Photocatalytic reduction of CO_2 on TiO_2 and other semiconductors. Angew. Chem. Int. Ed., 52 (2013), pp. 7372-7408.

[17] M. Muratori, H. Kheshgi, B. Mignone, L. Clarke, H. McJeon, J. Edmonds. Carbon capture and storage across fuels and sectors in energy system transformation pathways. Int. J. Greenh. Gas Control, 57 (2017), pp. 34-41.

[18] S. Das, W.M.A. Wan Daud. Photocatalytic CO_2 transformation into fuel: a review on advances in photocatalyst and photoreactor. Renew. Sustain. Energy Rev., 39 (2014), pp. 765-805.

[19] S.Y. Lee, J.U. Lee, I.B. Lee, J. Han. Design under uncertainty of carbon capture and storage infrastructure considering cost, environmental impact, and preference on risk. Appl. Energy, 189 (2017), pp. 725-738.

[20] R. Daiyan, X. Lu, Y.H. Ng, R. Amal. Liquid hydrocarbon production from CO_2: recent development in electrocatalysts. ChemSusChem (2017).

[21] F. Marpani, M. Pinelo, A.S. Meyer. Enzymatic conversion of CO_2 to CH_3OH via reverse dehydrogenase cascade biocatalysis: quantitative comparison of efficiencies of immobilized enzyme systems. Biochem. Eng. J., 127 (2017), pp. 217-228.

[22] Gao, C. Jia, B. Liu. Direct and selective hydrogenation of CO_2 to ethylene and propene by bifunctional catalysts. Catal. Sci. Technol. (2017).

[23] W. Tu, Y. Zhou, Z. Zou. Photocatalytic conversion of CO_2 into renewable hydrocarbon fuels: state-of-the-art accomplishment, challenges, and prospects. Adv. Mater., 26 (2014), pp. 4607-4626.

[24] T. Inoue, A. Fujishima, S. Konishi, K. Honda. Photoelectrocatalytic reduction of carbon dioxide in aqueous suspensions of semiconductor powders. Nature, 277 (1979), pp. 637-638.

[25] Z. Xiong, Z. Lei, Z. Xu, X. Chen, B. Gong, Y. Zhao, *et al.* Flame spray pyrolysis synthesized ZnO/CeO_2 nanocomposites for enhanced CO_2photocatalytic reduction under UV–Vis light irradiation. Biochem. Pharmacol., 18 (2017), pp. 53-61.

[26] Y. Yang, F. Zhan, H. Li, W. Liu, S. Yu. In situ sn-doped WO_3 films with enhanced photoelectrochemical performance for reducing CO_2 into formic acid. J. Solid State Electrochem., 21 (2017), pp. 2231-2240.

[27] T.P. Senftle, M. Lessio, E.A. Carter. Interaction of pyridine and water with the reconstructed surfaces

of GaP (111) and CdTe (111) photoelectrodes : implications for CO_2 reduction. Chem. Mater. (2016).

[28] Y. Pan, Z. Sun, H. Cong, Y. Men, S. Xin, J. Song, *et al.* Photocatalytic CO_2 reduction highly enhanced by oxygen vacancies on Pt-nanoparticle-dispersed gallium oxide. Nano Res., 9 (2016), pp. 1689-1700.

[29] C.C. Lo, C.H. Hung, C.S. Yuan, J.F. Wu. Photoreduction of carbon dioxide with H_2 and H_2O over TiO_2 and ZrO_2 in a circulated photocatalytic reactor. Sol. Energy Mater. Sol. Cells, 91 (2007), pp. 1765-1774.

[30] K. Koj, P. Praus, M. Edelmannová, N. Ambrožová, I. Troppová, D. Fridrichová, *et al.* Photocatalytic reduction of CO_2 Over CdS, ZnS and on montmorillonite. J. Nanosci. Nanotechnol., 17 (2017), pp. 4041-4047.

[31] K. Koˇ, P. Praus, M. Edelmannová, N. Ambrožová, I. Troppová, D. Fridrichová, *et al* .Photocatalytic reduction of CO_2 Over CdS, ZnS and on montmorillonite. J. Nanosci. Nanotechnol., 17 (2017), pp. 4041-4047.

[32] Y. Wang, F. Xin, J. Chen, T. Xiang. Photocatalytic reduction of CO_2 in isopropanol on Bi_2S_3 quantum dots/TiO_2 nanosheets with exposed {001} facets. J. Nanosci. Nanotechnol., 17 (2017), pp. 1863-1869.

[33] A. Ali, W. Oh. A simple ultrasono-synthetic route of PbSe- graphene-TiO_2 ternary composites to improve the photocatalytic reduction of CO_2.Fuller. Nanotub. Carbon Nanostruct., 25 (2017), pp. 449-458.

[34] T. Ohno, N. Murakami, T. Koyanagi, Y. Yang. Photocatalytic reduction of CO_2 over a hybrid photocatalyst composed of WO_3 and graphitic carbon nitride (g-C_3N_4) under visible light. J. CO_2 Util., 6 (2014), pp. 17-25.

[35] M. Reli, M. Kobielusz, L. Matìjová, S. Daniš, W. Macyk, L. Obalová, *et al.*TiO_2 processed by pressurized hot solvents as a novel photocatalyst for photocatalytic reduction of carbon dioxide. Appl. Surf. Sci., 391 (2017), pp. 282-287.

[36] M. Tahir, N.S. Amin. Advances in visible light responsive titanium oxide-based photocatalysts for CO_2conversion to hydrocarbon fuels. Energy Convers. Manag., 76 (2013), pp. 194-214.

[37] S. Nahar, M. Zain, A. Kadhum, H. Hasan, M. Hasan. Advances in photocatalytic CO_2 reduction with water: a review. Mater. (Basel), 10 (2017), pp. 629-655.

[38] A. Corma, H. Garcia. Photocatalytic reduction of CO_2 for fuel production: possibilities and challenges. J. Catal., 308 (2013), pp. 168-175.

[39] Y. Sohn, W. Huang, F. Taghipour. Recent progress and perspectives in the photocatalytic CO_2 reduction of Ti-oxide-based nanomaterials. Appl. Surf. Sci., 396 (2016), pp. 1696-1711.

[40] D. Pei, J. Luan. Development of visible light-responsive sensitized photocatalysts. Int. J. Photoenergy, 2012 (2012).

[41] J.L. White, M.F. Baruch, J.E. Pander, Y. Hu, I.C. Fortmeyer, J.E. Park, *et al.* Light-driven heterogeneous reduction of carbon dioxide: photocatalysts and photoelectrodes. Chem. Rev., 115 (2015), pp. 12888-12935.

[42] W.N. Wang, J. Soulis, Y. Jeffrey Yang, P. Biswas. Comparison of CO_2 photoreduction systems: a review. Aerosol. Air Qual. Res., 14 (2014), pp. 533-549.

[43] X. Chang, T. Wang, J. Gong. CO_2 photo-reduction: insights into CO_2 activation and reaction on surfaces of photocatalysts. Energy Environ. Sci., 9 (2016), pp. 2177-2196.

[44] K.S. Novoselov, A.K. Geim, S.V. Morozov, Jiang D., Zhang Y., S.V. Dubonos, I.V. Grigorieva, A.A.Firsov. Electric field effect in atomically thin carbon films. Science, 306 (5696) (2004), pp. 666-669.

[45] J.C. Meyer, A.K. Geim, M.I. Katsnelson, K.S. Novoselov, T.J. Booth, S. Roth. The structure of suspended graphene sheets. Nature, 446 (2007), pp. 60-63.

[46] B. Mensah, K.C. Gupta, Kim H., Wang W., Jeong K.-U., Nah C.Graphene- reinforced elastomeric nanocomposites: a review. Polym Test, 68 (2018), pp. 160-184.

[47] Ren S., Rong P., Yu Q.Preparations, properties and applications of graphene in functional devices: a concise review. Ceram Int, 44 (11) (2018), pp. 11940-11955.

[48] Hiew B.Y.Z., Lee L.Y., Lee X.J., S. ThangalazhyGopakumar, Gan S., Lim S.S., Pan G.T., YangT.C.-K.,

Chiu W.S., Khiew P.S.Review on synthesis of 3D graphene-based configurations and their adsorption performance for hazardous water pollutants. Process Saf Environ, 116 (2018), pp. 262-286.

[49] B.L. Dasari, J.M. Nouri, D. Brabazon, S. Naher. Graphene and derivatives – Synthesis techniques, properties and their energy applications. Energy, 140 (2017), pp. 766-778.

[50] Zhao L., Yu B., Xue F., Xie J., Zhang X., Wu R., Wang R., Hu Z., Yang S.-T., Luo J.Facile hydrothermal preparation of recyclable S-doped graphene sponge for Cu^{2+}adsorption. J Hazard Mat, 286 (2015), pp. 449-456.

[51] Yang W, Zhao Q, Xin L, Qiao J, Zou J, Shao P, Yu Z, Zhang Q, Wu G. Microstructure and mechanical properties of graphene nanoplates reinforced pure Al matrix composites prepared by pressure infiltration method. J Alloy Compd, 732 (2018), pp. 748-758.

[52] Ren S., Rong P., Yu Q. Preparations, properties and applications of graphene in functional devices: a concise review. Ceram Int, 44 (11) (2018), pp. 11940-11955.

[53] B.L. Dasari, J.M. Nouri, D. Brabazon, S. Naher. Graphene and derivatives – Synthesis techniques, properties and their energy applications. Energy, 140 (2017), pp. 766-778.

[54] K.S. Novoselov, A.K. Geim, S.V. Morozov, Jiang D., Zhang Y., S.V. Dubonos, I.V. Grigorieva, A.A.Firsov. Electric field effect in atomically thin carbon films. Science, 306 (5696) (2004), pp. 666-669.

[55] P. Bhawal, S. Ganguly, T.K. Chaki, N.C. Das. Synthesis and characterization of graphene oxide filled ethylene methyl acrylate hybrid nanocomposites. RSC Adv, 6 (2016), pp. 20781-20790.

[56] T. Szabó, O. Berkesi, P. Forgó, K. Josepovits, Y. Sanakis, D. Petridis, I. Dékány. Evolution of surface functional groups in a series of progressively oxidized graphite oxides. Chem Mater, 18 (11) (2006), pp. 2740-2749.

[57] Wang S., Sun H., Ang H.M., M.O. Tadé. Adsorptive remediation of environmental pollutants using novel graphene-based nanomaterials. Chem Eng J, 226 (2013), pp. 336-347.

[58] R.S. Edwards, K.S. Coleman. Graphene synthesis: relationship to applications. Nanoscale, 5 (1) (2013), pp. 38-51.

[59] A. Ambrosi, Chua C.K., A. Bonanni, M. Pumera. Electrochemistry of graphene and related materials. Chem Rev, 114 (2014), pp. 7150-7188.

[60] K.S. Novoselov, A.K. Geim, S.V. Morozov, Jiang D., Zhang Y., S.V. Dubonos, I.V. Grigorieva, A.A.Firsov. Electric field effect in atomically thin carbon films. Science, 306 (5696) (2004), pp. 666-669.

[61] Wu X., Liu Y., Yang H., Shi Z. Large-scale synthesis of high-quality graphene sheets by an improved alternating current arc-discharge method. RSC Adv, 6 (2016), pp. 93119-93124.

[62] Chua C.K., M. Pumera. Chemical reduction of graphene oxide: a synthetic chemistry viewpoint. Chem Soc Rev, 43 (1) (2014), pp. 291-312.

[63] T.F. Emiru, D.W. Ayele. Controlled synthesis, characterization and reduction of graphene oxide: a convenient method for large scale production. Egypt J Basic Appl Sci, 4 (2017), pp. 74-79.

[64] Ö. Güler, S.H. Güler, V. Selen, M.G. Albayrak, E. Evin. Production of graphene layer by liquid-phase exfoliation with low sonication power and sonication time from synthesized expanded graphite. Fuller Nanotubes Carbon Nanostruct, 24 (2016), pp. 123-127.

[65] S. Haar, M. Bruna, Lian J.X., F. Tomarchio, Y. Olivier, R. Mazzaro, *et al.* Liquid-phase exfoliation of graphite into single- and few-layer graphene with á-functionalized alkanes. J Phys Chem Lett, 7 (2016), pp. 2714-2721.

[66] Wu X., Liu Y., Yang H., Shi Z. Large-scale synthesis of high-quality graphene sheets by an improved alternating current arc-discharge method. RSC Adv, 6 (2016), pp. 93119-93124.

[67] A.M. Dimiev, A. Khannanov, I. Vakhitov, A. Kiiamov, K. Shukhina, J.M. Tour. Revisiting the mechanism of oxidative unzipping of multiwall carbon nanotubes to graphene nanoribbons. ACS Nano, 12 (2018), pp. 3985-3993.

[68] R.M. Jacobberger, R. Machhi, J. Wroblewski, B. Taylor, A.L. Gillian-aniel, M.S. Arnold. Simple graphene

synthesis via chemical vapor deposition. J Chem Educ, 92 (2015), pp. 1903-1907.

[69] Son M., M.-H. Ham. Low-temperature synthesis of graphene by chemical vapor deposition and its applications. FlatChem, 5 (2017), pp. 40-49.

[70] Huang H., Chen S., Wee A.T.S., Chen W. 1 - Epitaxial growth of graphene on silicon carbide (SiC). Graphene: Woodhead Publishing (2014), pp. 3-26.

[71] G. Yazdi, T. Iakimov, R. Yakimova. Epitaxial graphene on SiC: a review of growth and characterization. Crystal, 6 (2016), p. 53.

[72] D. Albert, F. Michael. Substrate-free microwave synthesis of graphene: experimental conditions and hydrocarbon precursors. New J Phys, 12 (2010), Article 125013.

[73] Yang Y., Liu R., Wu J., Jiang X., Cao P., Hu X., Pan T., Qiu C., Yang J., Song Y., Wu D., Su Y. Bottom-up fabrication of graphene on silicon/silica substrate via a facile soft-hard template approach. Sci Rep, 5 (2015), p. 13480.

[74] V. Singh, Joung D., Zhai L., S. Das, S.I. Khondaker, S. Seal. Graphene based materials: past, present and future. Prog Mater Sci, 56 (2011), pp. 1178-1271.

[75] B. Jayasena, S. Subbiah. A novel mechanical cleavage method for synthesizing few-layer graphenes. Nanoscale Res Lett, 6 (1) (2011), p. 95.

[76] Yi M., Shen Z. A review on mechanical exfoliation for the scalable production of graphene. J Mater Chem A, 3 (22) (2015), pp. 11700-11715.

[77] Chen J., Duan M., Chen G. Continuous mechanical exfoliation of graphene sheets via three-roll mill. J Mater Chem, 22 (37) (2012), p. 19625.

[78] Chua C.K., M. Pumera. Chemical reduction of graphene oxide: a synthetic chemistry viewpoint. Chem Soc Rev, 43 (1) (2014), pp. 291-312.

[79] O. Jankovsky, S. HrdlickovaKuckova, M. Pumera, P. Simek, D. Sedmidubsky, Z. Sofer. Carbon fragments are ripped off from graphite oxide sheets during their thermal reduction. N J Chem, 38 (12) (2014), pp. 5700-5705.

[80] Yu H., Zhang B., C. Bulin, Li R., Xing R. High-efficient synthesis of graphene oxide based on improved hummers method. Sci Rep, 6 (2016), p. 36143.

[81] T. Somanathan, K. Prasad, K.K. Ostrikov, A. Saravanan, V.M. Krishna. Graphene oxide synthesis from agro waste. Nanomaterials, 5 (2015), pp. 826-834.

[82] Chen J., Yao B., Li C., Shi G. An improved Hummers method for eco-friendly synthesis of graphene oxide. Carbon, 64 (2013), pp. 225-229.

[83] Zhong Y.L., Tian Z., G.P. Simon, Li D. Scalable production of graphene via wet chemistry: progress and challenges. Mater Today, 18 (2) (2015), pp. 73-78.

[84] Chen J., Yao B., Li C., Shi G. An improved Hummers method for eco-friendly synthesis of graphene oxide. Carbon, 64 (2013), pp. 225-229.

[85] O. Jankovsky, S. HrdlickovaKuckova, M. Pumera, P. Simek, D. Sedmidubsky, Z. Sofer. Carbon fragments are ripped off from graphite oxide sheets during their thermal reduction. N J Chem, 38 (12) (2014), pp. 5700-5705.

[86] Li D., M.B. Muller, S. Gilje, R.B. Kaner, G.G. Wallace. Processable aqueous dispersions of graphene nanosheets. Nat Nanotechnol, 3 (2) (2008), pp. 101-105.

[87] J. Campos-Delgado, A.R. Botello-Méndez, G. Algara Siller, B. Hackens, T. Pardoen, U. Kaiser, M.S. Dresselhaus, J.-C. Charlier, J.-P. Raskin. CVD synthesis of mono- and few-layer graphene using alcohols at low hydrogen concentration and atmospheric pressure. Chem Phys Lett, 584 (2013), pp. 142-146.

[88] Min B.H., Kim D.W., Kim K.H., Choi H.O., Jang S.W., Jung H.-T. Bulk scale growth of CVD graphene on Ni nanowire foams for a highly dense and elastic 3D conducting electrode. Carbon, 80 (2014), pp.

446-452.

[89] Min B.H., Kim D.W., Kim K.H., Choi H.O., Jang S.W., Jung H.-T. Bulk scale growth of CVD graphene on Ni nanowire foams for a highly dense and elastic 3D conducting electrode. Carbon, 80 (2014), pp. 446-452.

[90] J. Campos-Delgado, A.R. Botello-Méndez, G. AlgaraSiller, B. Hackens, T. Pardoen, U. Kaiser, M.S. Dresselhaus, J.-C. Charlier, J.-P. Raskin. CVD synthesis of mono- and few-layer graphene using alcohols at low hydrogen concentration and atmospheric pressure. Chem Phys Lett, 584 (2013), pp. 142-146.

[91] Jang J., Son M., Chung S., Kim K., Cho C., Lee B.H., M.H. Ham. Low-temperature-grown continuous graphene films from benzene by chemical vapor deposition at ambient pressure. Sci Rep, 5 (2015), p. 17955.

[92] Kalita, M.E. Ayhan, S. Sharma, S.M. Shinde, D. Ghimire, K. Wakita, M. Umeno, M. Tanemura. Low temperature deposited graphene by surface wave plasma CVD as effective oxidation resistive barrier. Corros Sci, 78 (2014), pp. 183-187.

[93] V. Singh, Joung D., Zhai L., S. Das, S.I. Khondaker, S. Seal. Graphene based materials: past, present and future. Prog Mater Sci, 56 (2011), pp. 1178-1271.

[94] N. Mishra, J. Boeckl, N. Motta, F. Iacopi. Graphene growth on silicon carbide: a review (Phys. Status Solidi A 9"2016). Phys Status solidi (A), 213 (2016), pp. 2269-2289.

[95] N. Mishra, J. Boeckl, N. Motta, F. Iacopi. Graphene growth on silicon carbide: a review (Phys. Status Solidi A 9"2016). Phys Status solidi (A), 213 (2016), pp. 2269-2289.

[96] B. Gupta, M. Notarianni, N. Mishra, M. Shafiei, F. Iacopi, N. Motta. Evolution of epitaxial graphene layers on 3C SiC/Si (111) as a function of annealing temperature in UHV. Carbon, 68 (2014), pp. 563-572.

[97] C. Riedl, C. Coletti, U. Starke. Structural and electronic properties of epitaxial graphene on SiC(0 0 0 1): a review of growth, characterization, transfer doping and hydrogen intercalation. J Phys D Appl Phys, 43 (37) (2010), Article 374009.

[98] B. Gupta, M. Notarianni, N. Mishra, M. Shafiei, F. Iacopi, N. Motta. Evolution of epitaxial graphene layers on 3C SiC/Si (111) as a function of annealing temperature in UHV. Carbon, 68 (2014), pp. 563-572.

[99] V. Singh, Joung D., Zhai L., S. Das, S.I. Khondaker, S. Seal. Graphene based materials: past, present and future. Prog Mater Sci, 56 (2011), pp. 1178-1271.

[100] W. Norimatsu, M. Kusunoki. Epitaxial graphene on SiC[1]: advances and perspectives. Phys Chem Chem Phys, 16 (8) (2014), pp. 3501-3511.

[101] W. Norimatsu, M. Kusunoki. Epitaxial graphene on SiC[1]: advances and perspectives. Phys Chem Chem Phys, 16 (8) (2014), pp. 3501-3511.

[102] W. Norimatsu, M. Kusunoki. Epitaxial graphene on SiC[1]: advances and perspectives. Phys Chem Chem Phys, 16 (8) (2014), pp. 3501-3511.

[103] Choi W., I. Lahiri, R. Seelaboyina, Kang Y.S. Synthesis of graphene and its applications: a review. Crit Rev Solid State, 35 (1) (2010), pp. 52-71.

[104] Nhut J M, Pesant L, Tessonnier J P, Winé G, Guille J, Pham Huu C, Ledoux M J. Appl Catal A, 2003, 254: 345.

[105] Shi J W, Zheng Ji T, Wu P, Ji X J. Catal Commun, 2008, 9: 1846.

[106] Geim A K, Novoselov K S. Nat Mater, 2007, 6: 183.

[107] Li X, Zhao W F, Chen G H. Mater Rev, 2008, 22(8): 48.

[108] Oh W C, Chen M L, Cho K Y, Kim C Y, Meng Z, Zhu L. Chin J Catal, 2011, 32: 1577.

[109] Zhao H M, Su F, Fan X F, Yu H T, Wu D, Quan X. Chin J Catal, 2012, 33: 777.

[110] R. Long, N.J. English, O.V. Prezhdo. Photo-induced charge separation across the graphene–TiO_2

interface is faster than energy losses: a time-domain ab initio analysis. J. Am. Chem. Soc., 134 (2012), pp. 14238-14248.

[111] S. Chowdhury, R. Balasubramanian. Graphene/semiconductor nanocomposites (GSNs) for heterogeneous photocatalytic decolorization of wastewaters contaminated with synthetic dyes: a review. Appl. Catal. B, 160 (2014), pp. 307-324.

[112] S. Chowdhury, R. Balasubramanian. Graphene/semiconductor nanocomposites (GSNs) for heterogeneous photocatalytic decolorization of wastewaters contaminated with synthetic dyes: a review. Appl. Catal. B, 160 (2014), pp. 307-324.

[113] A.M. Jastrzêbska, J. Karcz, R. Letmanowski, D. Zabost, E. Ciecierska, M. Siekierski, A. Olszyna. Synthesis of RGO/TiO_2 nanocomposite flakes and characterization of their unique electrostatic properties using zeta potential measurements. J. Alloys Compd., 679 (2016), pp. 470-484.

[114] S. Liu, H. Sun, S. Liu, S. Wang. Graphene facilitated visible light photodegradation of methylene blue over titanium dioxide photocatalysts. Chem. Eng. J., 214 (2013), pp. 298-303.

[115] A. Sharma, B.-K. Lee. Rapid photo-degradation of 2-chlorophenol under visible light irradiation using cobalt oxide-loaded TiO_2/reduced graphene oxide nanocomposite from aqueous media. J. Environ. Manage., 165 (2016), pp. 1-10.

[116] X. Pan, M.-Q. Yang, Z.-R. Tang, Y.-J. Xu. Noncovalently functionalized graphene-directed synthesis of ultralarge graphene-based TiO_2 nanosheet composites: tunable morphology and photocatalytic applications. J. Phys. Chem. C., 118 (2014), pp. 27325-27335.

[117] J. Li, Q. Zhang, L. Zeng, D. He. Synthesis, characterization and photocatalytic study of graphene oxide and cerium co-doped in TiO_2. Appl. Phys. A, 122 (2016), p. 51.

[118] G. Dai, X. Wang, S. Liu, Y. Liang, K. Liu. Template-free fabrication of hierarchical macro-/mesoporous N-doped TiO_2/graphene oxide composites with enhanced visible-light photocatalytic activity. J. Chin. Chem. Soc., 62 (2015), pp. 170-176.

[119] M.R. Hasan, S.B. AbdHamid, W.J. Basirun, Z.Z. Chowdhury, A.E. Kandjani, S.K. Bhargava. Ga doped RGO–TiO_2 composite on an ITO surface electrode for investigation of photoelectrocatalytic activity under visible light irradiation. New J. Chem., 39 (2015), pp. 369-376.

[120] Y. Haldorai, A. Rengaraj, C.H. Kwak, Y.S. Huh, Y.-K. Han. Fabrication of nano TiO2@graphene composite: reusable photocatalyst for hydrogen production, degradation of organic and inorganic pollutants. Synth. Met., 198 (2014), pp. 10-18.

[121] A.P. Bhirud, S.D. Sathaye, R.P. Waichal, J.D. Ambekar, C.-J. Park, B.B. Kale. In-situ preparation of N-TiO_2/graphene nanocomposite and its enhanced photocatalytic hydrogen production by H_2S splitting under solar light. Nanoscale, 7 (2015), pp. 5023-5034.

[122] H.-H. Chun, W.-K. Jo. Adsorption and photocatalysis of 2-ethyl-1-hexanol over graphene oxide–TiO_2 hybrids post-treated under various thermal conditions. Appl. Catal. B, 180 (2016), pp. 740-750.

[123] J. Wei, S. Xue, P. Xie, R. Zou. Synthesis and photocatalytic properties of different SnO_2 microspheres on graphene oxide sheets. Appl. Surf. Sci., 376 (2016), pp. 172-179.

[124] D.K. Padhi, G.K. Pradhan, K.M. Parida, S.K. Singh. Facile fabrication of $Gd(OH)_3$ nanorod/RGO composite: synthesis, characterization and photocatalytic reduction of Cr(VI). Chem. Eng. J., 255 (2014), pp. 78-88.

[125] Y. Wang, Z. Mo, P. Zhang, C. Zhang, L. Han, R. Guo, H. Gou, X. Wei, R. Hu. Synthesis of flower-like TiO_2 microsphere/graphene composite for removal of organic dye from water. Mater. Des., 99 (2016), pp. 378-388.

[126] A. Trapalis, N. Todorova, T. Giannakopoulou, N. Boukos, T. Speliotis, D. Dimotikali, J. Yu. TiO_2/graphene composite photocatalysts for NOx removal: a comparison of surfactant-stabilized graphene and reduced graphene oxide. Appl. Catal. B, 180 (2016), pp. 637-647.

[127] M.S. Sher Shah, K. Zhang, A.R. Park, K.S. Kim, N.-G. Park, J.H. Park, P.J. Yoo. Single-step solvothermal synthesis of mesoporous Ag–TiO_2–reduced graphene oxide ternary composites with enhanced

photocatalytic activity. Nanoscale, 5 (2013), pp. 5093-5101.

[128] L. Liu, Z. Liu, A. Liu, X. Gu, C. Ge, F. Gao, L. Dong. Engineering the TiO_2-graphene interface to enhance photocatalytic H_2 production. ChemSusChem, 7 (2014), pp. 618-626.

[129] S. Thangavel, K. Krishnamoorthy, S.-J. Kim, G. Venugopal. Designing ZnS decorated reduced graphene-oxide nanohybrid via microwave route and their application in photocatalysis. J. Alloys Compd., 683 (2016), pp. 456-462.

[130] S. Cao, T. Liu, Y. Tsang, C. Chen. Role of hydroxylation modification on the structure and property of reduced graphene oxide/TiO_2 hybrids. Appl. Surf. Sci., 382 (2016), pp. 225-238.

[131] S. Chowdhury, R. Balasubramanian. Graphene/semiconductor nanocomposites (GSNs) for heterogeneous photocatalytic decolorization of wastewaters contaminated with synthetic dyes: a review. Appl. Catal. B, 160 (2014), pp. 307-324.

[132] A.N. Fouda, E.S.M. Duraia. Self-assembled graphene oxide on a photo-catalytic active transparent conducting oxide. Mater. Des., 90 (2016), pp. 284-290.

[133] C. Xu, J. Zhu, R. Yuan, X. Fu. More effective use of graphene in photocatalysis by conformal attachment of small sheets to TiO_2 spheres. Carbon, 96 (2016), pp. 394-402.

[134] W. Xiao, Y. Zhang, L. Tian, H. Liu, B. Liu, Y. Pu. Facile synthesis of reduced graphene oxide/titania composite hollow microspheres based on sonication-assisted interfacial self-assembly of tiny graphene oxide sheets and the photocatalytic property. J. Alloys Compd., 665 (2016), pp. 21-30.

[135] W.-N. Wang, Y. Jiang, J.D. Fortner, P. Biswas. Nanostructured graphene-titanium dioxide composites synthesized by a single-step aerosol process for photoreduction of carbon dioxide. Environ. Eng. Sci., 31 (2014), pp. 428-434.

[136] B. Luo, G. Liu, L. Wang. Recent advances in 2D materials for photocatalysis. Nanoscale, 8 (2016), pp. 6904-6920.

[137] X. Luan, M.T. Gutierrez Wing, Y. Wang. Enhanced photocatalytic activity of graphene oxide/titania nanosheets composites for methylene blue degradation. Mater. Sci. Semicond. Process., 30 (2015), pp. 592-598.

[138] M. Zeng, W.-L. Wang, X.-D. Bai. Preparing three-dimensional graphene architectures: review of recent developments. Chin. Phys. B, 22 (98105) (2013).

[139] R. Fang, X. Ge, M. Du, Z. Li, C. Yang, B. Fang, Y. Liang. Preparation of silver/graphene/polymer hybrid microspheres and the study of photocatalytic degradation. Colloid. Polym. Sci., 292 (2014), pp. 985-990.

[140] A Fujishima, K Honda. Electrochemical photolysis of water at a semiconductor electrode. Nature, 238 (1972), pp. 37-38.

[141] Li R, Weng Y, Zhou X, Wang X, Mi Y, Chong R, *et al.* Achieving overall water splitting using titanium dioxide-based photocatalysts of different phases. Energy Environ Sci, 8 (2015), pp. 2377-2382.

[142] MF Ehsan, R Khan, He T. Visible Light photoreduction of CO_2 into CH_4 over ZnTe modified TiO_2 coral like nanostructures. ChemPhysChem, 18 (2017), pp. 3203-3210.

[143] Wang S, Hai X, Ding X, Chang K, Xiang Y, Meng X, *et al.*Light Switchable oxygen vacancies in ultrafine Bi_5O_7Br nanotubes for boosting solar driven nitrogen fixation in pure water. Adv Mater, 29 (2017), p. 170774.

[144] Chen X, Li N, Kong Z, Ong W-J, Zhao X. Photocatalytic fixation of nitrogen to ammonia: state-of-the-art advancement and future prospects. Mater Horiz, 5 (2018), pp. 9-27.

[145] Guo Z, Ma R, Li G. Degradation of phenol by nanomaterial TiO_2 in wastewater. Chem Eng J, 119 (2006), pp. 55-59.

[146] Elizabeth A. Jones. Semiconductor Physics and Devices.

[147] J. Low, S. Cao, J. Yu, S. Wageh. Two-dimensional layered composite photocatalysts. Chem. Commun.,

50 (2014), pp. 10768-10777.

[148] F. Xiang, R. Mukherjee, J. Zhong, Y. Xia, N. Gu, Z. Yang, N. Koratkar. Scalable and rapid far infrared reduction of graphene oxide for high performance lithium ion batteries. Energy Storage Mater., 1 (2015), pp. 9-16.

[149] M. Yu, R. Li, M. Wu, G. Shi. Graphene materials for lithium–sulfur batteries. Energy Storage Mater., 1 (2015), pp. 51-73.

[150] Y. Zhou, X. Xu, B. Shan, Y. Wen, T. Jiang, J. Lu, S. Zhang, D.P. Wilkinson, J. Zhang, Y. Huang. Tuning and understanding the super capacitance of heteroatom-doped graphene. Energy Storage Mater., 1 (2015), pp. 103-111.

[151] Q. Wang, J. Yan, Z. Dong, L. Qu, Z. Fan. Densely stacked bubble-pillared graphene blocks for high volumetric performance supercapacitors. Energy Storage Mater., 1 (2015), pp. 42-50.

[152] M. Li, W. Guo, H. Li, S. Xu, C. Qu, B. Yang. Synthesis of chemical vapor deposition graphene on tantalum wire for supercapacitor applications. Appl. Surf. Sci., 317 (2014), pp. 1100-1106.

[153] Y.S. Kang, N. Jung, K.H. Choi, M.J. Lee, M. Ahn, Y.H. Cho, Y.E. Sung. Anode electrode with carbon buffer layer for improving methanol oxidation reaction in direct methanol fuel cell. Appl. Surf. Sci., 290 (2014), pp. 246-251.

[154] Y. Fu, J. Yu, Y. Zhang, Y. Meng. Graphite coated with manganese oxide/multiwall carbon nanotubes composites as anodes in marine benthic microbial fuel cells. Appl. Surf. Sci., 317 (2014), pp. 84-89.

[155] Y. Li, B.P. Zhang, J.X. Zhao, Z.H. Ge, X.K. Zhao, L. Zou. ZnO/carbon quantum dots heterostructure with enhanced photocatalytic properties. Appl. Surf. Sci., 279 (2013), pp. 367-373.

[156] S. Hu, Y. Ding, Q. Chang, J. Yang, K. Lin. Chlorine-functionalized carbon dots for highly efficient photodegradation of pollutants under visible-light irradiation. Appl. Surf. Sci., 355 (2015), pp. 774-777.

[157] K.S. Novoselov, A.K. Geim, S.V. Morozov, D. Jiang, Y. Zhang, S.V. Dubonos, I.V. Grigorieva, A.A.Firsov. Electric field effect in atomically thin carbon films. Science, 306 (2004), pp. 666-669.

[158] L.K. Putri, W.J. Ong, W.S. Chang, S.P. Chai. Heteroatom doped graphene in photocatalysis: a review. Appl. Surf. Sci., 358 (2015), pp. 2-14.

[159] J.X. Low, J.G. Yu, W.K. Ho. Graphene-based photocatalysts for CO_2 reduction to solar fuel. J. Phys. Chem. Lett., 6 (2015), pp. 4244-4251.

[160] Y. Zhang, B. Shen, H. Huang, Y. He, B. Fei, F. Lv. $BiPO_4$/reduced graphene oxide composites photocatalyst with high photocatalytic activity. Appl. Surf. Sci., 319 (2014), pp. 272-277.

[161] Y.T. Liang, B.K. Vijayan, O. Lyandres, K.A. Gray, M.C. Hersam. Effect of dimensionality on the photocatalytic behavior of carbon-titania nanosheet composites: charge transfer at nanomaterial interfaces. J. Phys. Chem. Lett., 3 (2012), pp. 1760-1765.

[162] Q.J. Xiang, J.G. Yu. Graphene-based photocatalysts for hydrogen generation. J. Phys. Chem. Lett., 4 (2013), pp. 753-759.

[163] E.S. Baeissa. Green synthesis of methanol by photocatalytic reduction of CO_2 under visible light using a graphene and tourmaline co-doped titania nanocomposites. Ceram. Int., 40 (2014), pp. 12431-12438.

[164] J.I. Pankove. Optical Processes in Semiconductors. Courier Corporation (2012).

[165] K. Rajeshwar, R. McConnell, S. Licht (Eds.), Solar Hydrogen Generation: Toward a Renewable Energy Future, Kluwer Academic, New York (2008).

[166] K. Rajeshwar. Fundamentals of semiconductor electrochemistry and photoelectrochemistry. A.J. Bard, M. Stratmann, S. Licht (Eds.), Encyclopedia of Electrochemistry, Volume 6, Semiconductor Electrodes and Photoelectrochemistry, Wiley-VCH, Weinheim (2002), pp. 3-53.

[167] H.-J. Lewerenz, L.M. Peter (Eds.), Photoelectrochemical Water Splitting: Issues and Perspectives, Royal Society of Chemistry London (2013).

[168] A. Kormányos, A. Thomas, M.N. Huda, P. Sarker, J. PingLiu, N. Poudyal, C. Janáky, K.Rajeshwar. J. Phys. Chem. C, 120 (2016), pp. 16024-16034.

[169] C. Janaky, D. Hursán, B. Endrõdi, W. Chanmanee, D. Roy, D. Liu, N.R. de Tacconi, B.H. Dennis, K. Rajeshwar. ACS Energy Lett., 1 (2016), pp. 332-338.

[170] A. Thomas, G.F. Samu, M.N. Huda, P. Sarker, J.P. Liu, V. Nguyen, E. Wang, K.A. Schug, K.Rajeshwar. ChemSusChem, 8 (2015), pp. 1652-1663.

[171] G. F. Samu, A. Veres, B. Endrodi, E. Varga, K. Rajeshwar, C. Janaky, to be published (2016).

[172] M. Reli, M. Kobielusz, L. Matìjová, S. Daniš, W. Macyk, L. Obalová, *et al.* TiO_2 processed by pressurized hot solvents as a novel photocatalyst for photocatalytic reduction of carbon dioxide. Appl. Surf. Sci., 391 (2017), pp. 282-287.

[173] J. Jiao, Y. Wei, K. Chi, Z. Zhao, A. Duan, J. Liu. Platinum nanoparticles supported on TiO_2 photonic crystals as highly active photocatalyst for the reduction of CO_2 in the presence of water. Energy Technol., 5 (2017), pp. 877-883.

[174] J.-L. Gong, B. Wang, G.-M. Zeng, C.-P. Yang, C.-G. Niu, Q.-Y. Niu, W. J. Zhou, Y. Liang. J. Hazard. Mater., 164 (2009), pp. 1517-1522.

[175] X. Li, J. Yu, S. Wageh, A.A. Al-Ghamdi, J. Xie. Small, 12 (2016), pp. 6640-6696.

[176] D. Huang, X. Wang, C. Zhang, G. Zeng, Z. Peng, J. Zhou, M. Cheng, R. Wang, Z. Hu, X. Qin. Chemosphere, 186 (2017), pp. 414-421.

[177] J. Wang, Z. Yang, X. Gao, W. Yao, W. Wei, X. Chen, R. Zong, Y. Zhu. Appl. Catal. B: Environ., 217 (2017), pp. 169-180.

[178] X. Chen, Q. Chen, W. Jiang, Z. Wei, Y. Zhu. Appl. Catal. B: Environ., 211 (2017), pp. 106-113.

[179] W. Chen, Y.-X. Hua, Y. Wang, T. Huang, T.-Y. Liu, X.-H. Liu. J. Catal., 349 (2017), pp. 8-18

[180] C.Y. Zhou, C. Lai, D.L. Huang, G.M. Zeng, C. Zhang, M. Cheng, L. Hu, J. Wan, W.P. Xiong, M.Wen, X.F. Wen, L. Qin. Appl. Catal. B: Environ., 220 (2018), pp. 202-210.

[181] A Fujishima, K Honda. Electrochemical photolysis of water at a semiconductor electrode. Nature, 238 (1972), pp. 37-38.

[182] M Yoshida, A Yamakata, K Takanabe, J Kubota, M Osawa, K Domen. ATR-SEIRAS investigation of the Fermi level of Pt cocatalyst on a GaN photocatalyst for hydrogen evolution under irradiation. J Am Chem Soc, 131 (2009), p. 13218.

[183] FE Osterloh. Inorganic materials as catalysts for photochemical splitting of water. Chem Mater, 20 (2008), pp. 35-54.

[184] Tsuji I, H Kato, A Kudo. Visible light induced H_2 evolution from an aqueous solution containing sulfide and sulfite over a ZnS–$CuInS_2$–$Evolu_2$ solid solution photocatalyst. Angew Chem Int Ed, 44 (2005), pp. 3565-3568.

[185] H Kato, H Kobayashi, A Kudo. Role of Ag^+ in the band structures and photocatalytic properties of $AgMO_3$ (M: Ta and Nb) with the perovskite structure. J Phys Chem B, 106 (2002), pp. 12441-12447.

[186] Tsuji I, A Kudo. H_2 evolution from aqueous sulfite solutions under visible-light irradiation over Pb and halogen-codoped ZnS photocatalysts. J Photochem Photobiol A Chem, 156 (2003), pp. 249-252.

[187] Hosogi Y, H Kato, A Kudo. Visible light response of $AgLi_{1/3}M_{2/3}O_2$ (M= Ti and Sn) synthesized from layered Li_2MO_3using molten $AgNO_3$. J Mater Chem, 18 (2008), pp. 647-653.

[188] Noji T, Jin T, Nango M, N Kamiya, Y Amao. CO_2 Photoreduction by formate dehydrogenase and a Ru-complex in a nanoporous glass reactor. ACS Appl Mater Interfaces, 9 (2017), pp. 3260-3265.

[189] Chen H, Shen K, Chen J, Chen X, Li Y. Hollow-ZIF-templated formation of a ZnO@ C–N–Co core–shell nanostructure for highly efficient pollutant photodegradation. J Mater Chem A (2017).

[190] Noji T, Jin T, Nango M, N Kamiya, Y Amao. CO_2 Photoreduction by formate dehydrogenase and a Ru-complex in a nanoporous glass reactor. ACS Appl Mater Interfaces, 9 (2017), pp. 3260-3265.

[191] SU Khan, M Al-Shahry, WB Ingler. Efficient photochemical water splitting by a chemically modified n-TiO_2. Science., 297 (2002), pp. 2243-2245.

[192] M Yoshida, A Yamakata, K Takanabe, J Kubota, M Osawa, K Domen. ATR-SEIRAS investigation of the Fermi level of Pt cocatalyst on a GaN photocatalyst for hydrogen evolution under irradiation. J Am Chem Soc, 131 (2009), p. 13218.

[193] M Murdoch, GIN Waterhouse, MA Nadeem, JB Metson, MA Keane, RF Howe, *et al.* The effect of gold loading and particle size on photocatalytic hydrogen production from ethanol over Au/TiO, nanoparticles. Nat Chem, 3 (2011), p. 489.

[194] J Hirayama, Y Kamiya. Highly selective and efficient photocatalytic reduction of nitrate in water by a tandem reaction system consisting of Pt/TiO_2 and $SnPd/Al_2O_3$: a comparative study of the tandem reaction system with a typical semiconductor photocatalyst, $SnPd/TiO_2$ J Catal, 348 (2017), pp. 306-313.

[195] Mecherikunnel AT, Richmond J. Spectral distribution of solar radiation. 1980.

[196] Wang X, K Maeda, A Thomas, K Takanabe, Xin G, JM Carlsson, *et al.* A metal-free polymeric photocatalyst for hydrogen production from water under visible light. Nat. Mater, 8 (2009), pp. 76-80.

[197] J. Song, X. Wang, C.-T. Chang. Preparation and characterization of graphene oxide. J. Nanomater., 2014 (2014), pp. 1-6.

[198] X. An, J.C. Yu. Graphene-based photocatalytic composites. RSC Adv., 1 (2011), pp. 1426-1434.

[199] N. Zhang, Y. Zhang, Y.-J. Xu. Recent progress on graphene-based photocatalysts: current status and future perspectives. Nanoscale, 4 (2012), pp. 5792-5813.

[200] E.V. Kondratenko, G. Mul, J. Baltrusaitis, G.O. Larrazabal, J. Perez-Ramirez. Energy Environ. Sci., 6 (2013), pp. 3112-3135.

[201] S.N. Habisreutinger, L. Schmidt-Mende, J.K. Stolarczyk. Angew. Chem. Int. Ed., 52 (2013), pp. 7372-7408.

[202] C. Gao, Q. Meng, K. Zhao, H. Yin, D. Wang, J. Guo, S. Zhao, L. Chang, M. He, Q. Li, H. Zhao, X.Huang, Y. Gao, Z. Tang. Adv. Mater., 28 (2016), pp. 6485-6490.

[203] Y. Wang, L. Zhang, X. Zhang, Z. Zhang, Y. Tong, F. Li, J.C.S. Wu, X. Wang. Appl. Catal. B Environ., 206 (2017), pp. 158-167.

[204] H. Xu, S. Ouyang, P. Li, T. Kako, J. Ye. ACS Appl. Mater. Interfaces, 5 (2013), pp. 1348-1354.

[205] X. Meng, Q. Yu, G. Liu, L. Shi, G. Zhao, H. Liu, P. Li, K. Chang, T. Kako, J. Ye. Nano Energy, 34 (2017), pp. 524-532.

[206] Y.S. Chaudhary, T.W. Woolerton, C.S. Allen, J.H. Warner, E. Pierce, S.W. Ragsdale, F.A.Armstrong. Chem. Commun., 48 (2012), pp. 58-60.

[207] L. Yu, G.J. Li, X.S. Zhang, X. Ba, G.D. Shi, Y. Li, P.K. Wong, J.C. Yu, Y. Yu. ACS Catal., 6 (2016), pp. 6444-6454.

[208] E.E. Barton, D.M. Rampulla, A.B. Bocarsly. J. Am. Chem. Soc., 130 (2008), pp. 6342-6344.

[209] A. Bachmeier, S. Hall, S.W. Ragsdale, F.A. Armstrong. J. Am. Chem. Soc., 136 (2014), pp. 13518-13521.

[210] S. Gao, Y. Lin, X. Jiao, Y. Sun, Q. Luo, W. Zhang, D. Li, J. Yang, Y. Xie. Nature, 529 (2016), pp. 68-71.

[211] Y. Wang, L. Zhang, X. Zhang, Z. Zhang, Y. Tong, F. Li, J.C.S. Wu, X. Wang. Appl. Catal. B Environ., 206 (2017), pp. 158-167.

[212] J. Cheng, M. Zhang, G. Wu, X. Wang, J. Zhou, K. Cen. Environ. Sci. Technol., 48 (2014), pp. 7076-7084.

[213] S. Neatu, J.A. Macia-Agullo, P. Concepcion, H. Garcia. J. Am. Chem. Soc., 136 (2014), pp. 15969-15976.

[214] Y. Zhang, B. Han, Y. Xu, D. Zhao, Y. Jia, R. Nie, Z. Zhu, F. Chen, J. Wang, H. Jing. ChemSusChem, 10 (2017), pp. 1742-1748.

[215] N.S. Lewis, D.G. Nocera, Proc. Natl. Acad. Sci. U.S.A. 103 (2006) 15729–15735.

[216] B. Kumar, J.M. Smieja, C.P. Kubiak, J. Phys. Chem. C 114 (2010) 14220–14223.

[217] J.M. Smieja, E.E. Benson, B. Kumar, K.A. Grice, C.S. Seu, A.J.M. Miller, J.M. Mayer,C.P. Kubiak, Proc. Natl. Acad. Sci. U.S.A. 109 (2012) 15646–15650.

[218] S. Kaneco, H. Katsumata, T. Suzuki, K. Ohta, Appl. Catal. B 64 (2006) 139–145

[219] Y. Zhang, B. Han, Y. Xu, D. Zhao, Y. Jia, R. Nie, Z. Zhu, F. Chen, J. Wang, H. Jing. ChemSusChem, 10 (2017), pp. 1742-1748.

[220] J. Cheng, M. Zhang, G. Wu, X. Wang, J. Zhou, K. Cen. Environ. Sci. Technol., 48 (2014), pp. 7076-7084.

[221] Y. Zhang, B. Han, Y. Xu, D. Zhao, Y. Jia, R. Nie, Z. Zhu, F. Chen, J. Wang, H. Jing. ChemSusChem, 10 (2017), pp. 1742-1748.

[222] J.L. White, M.F. Baruch, J.E. Pander Iii, Y. Hu, I.C. Fortmeyer, J.E. Park, T. Zhang, K. Liao, J. Gu, Y. Yan, T.W. Shaw, E. Abelev, A.B. Bocarsly. Chem. Rev., 115 (2015), pp. 12888-12935.

[223] Y. Qiu, F. Guo, R. Hurt, I. Külaots. Explosive thermal reduction of graphene oxide-based materials: mechanism and safety implications. Carbon, 72 (2014), pp. 215-223.

[224] L. Zeng, Z. Lu, M.H. Li, J. Yang, W.L. Song, D.W. Zeng, C.S. Xie, A modular calcination method to prepare modified N-doped TiO2 nanoparticle with high photocatalytic activity, Appl Catal. B-Environ. 183 (2016) 308–316.

[225] L. Song, X.Y. Zhao, L.X. Cao, J.W. Moon, B.H. Gu, W. Wang, Synthesis of rare earth doped TiO2 nanorods as photocatalysts for lignin degradation, Nanoscale 7 (2015). 16695–16703.

[226] Y.T. Liang, B.K. Vijayan, K.A. Gray, M.C. Hersam, Minimizing graphene defects enhance titania nanocomposite-based photocatalytic reduction of CO2 for improved solar fuel production, Nano Lett. 11 (2011) 2865–2870.

[227] S.S. Patil, M.G. Mali, M.S. Tamboli, D.R. Patil, M.V. Kulkarni, H. Yoon, H. Kim, S.S. Al-Deyab, S.S. Yoon, S.S. Kolekar, B.B. Kale, Green approach for hierarchical nanostructured Ag-ZnO and their photocatalytic performance under sunlight, Catal. Today 260 (2016) 126–134.

[228] Y. Wang, F. Xin, J. Chen, T. Xiang. Photocatalytic reduction of CO_2 in isopropanol on Bi_2S_3 quantum dots/TiO_2 nanosheets with exposed {001} facets J. Nanosci. Nanotechnol., 17 (2017), pp. 1863-1869.

[229] L. Liu, C. Zhao, J.T. Miller, Y. Li. Mechanistic study of CO_2 photoreduction with H_2O on Cu/TiO_2 nanocomposites by in situ x-ray absorption and infrared spectroscopies. J. Phys. Chem. C, 121 (2016), pp. 490-49.

[230] S. Krejèíková, L. Matìjová, K. Koèí, L. Obalová, Z. Matìj, L. Èapek, *et al.* Preparation and characterization of Ag-doped crystalline titania for photocatalysis applications. Appl. Catal. B: Environ., 111–112 (2012).

[231] F. Galli, M. Compagnoni, D. Vitali, C. Pirola, C.L. Bianchi, A. Villa, *et al.* CO_2 photoreduction at high pressure to both gas and liquid products over titanium dioxide. Appl. Catal. B: Environ., 200 (2017), pp. 386-391.

[232] Y. Li, W.-N. Wang, Z. Zhan, M.-H. Woo, C.-Y. Wu, P. Biswas. Photocatalytic reduction of CO_2 with H_2O on mesoporous silica supported Cu/TiO_2catalysts. Appl. Catal. B: Environ., 100 (2010), pp. 386-392.

[233] L. Collado, A. Reynal, J.M. Coronado, D.P. Serrano, J.R. Durrant, O. De la Peña, V.A. Shea. Effect of Au surface plasmon nanoparticles on the selective CO_2 photoreduction to CH_4. Appl. Catal. B: Environ., 178 (2015), pp. 177-185.

[234] K. Thamaraiselvi, T. Sivakumar. Photocatalytic reduction of carbon dioxide by using Bare and copper oxide impregnated nano titania catalysts. J. Nanosci., 17 (2017), pp. 313-322.

[235] W. Wang, D. Xu, B. Cheng, J. Yu, C. Jiang. Hybrid carbon@ TiO_2 hollow spheres with enhanced photocatalytic CO_2 reduction activity. J. Mater. Chem., 5 (2017), pp. 5020-5029

[236] B. Tahir, M. Tahir, N. Amin. Photocatalytic carbon dioxide and methane reduction to fuels over la-promoted titanium dioxide nanocatalyst. Chem. Eng., 56 (2017), pp. 1123-1128.

[237] C. Dong, M. Xing, J. Zhang. Economic hydrophobicity triggering of CO_2 photoreduction for selective CH_4 generation on noble-metal-free TiO_2-SiO_2. J. Phys. Chem. Lett., 7 (2016), pp. 2962-2966.

[238] J. Yu, J. Low, W. Xiao, P. Zhou, M. Jaroniec. Enhanced photocatalytic CO_2 -Reduction activity of anatase TiO_2 by co-exposed {001} and {101} facets. J. Am. Chem. Soc., 136 (2014), pp. 8839-8842.